ANALYSIS & DESIGN OF ACTIVE INDUCTOR

A Thesis

by

DIBYENDU RANA

Submitted to the Office of Graduate and Professional Studies of
Texas A&M University
in partial fulfillment of the requirements for the degree of

MASTER OF SCIENCE

Chair of Committee,	Prasad Enjeti
Committee Members,	Shankar Bhattacharyya
	Robert Balog
	Won-Jong Kim
Head of Department,	Chanan Singh

May 2014

Major Subject: Electrical Engineering

ABSTRACT

Power conditioning topologies such as adjustable speed drives (ASDs) have a growing demand in industry for improving efficiency and reducing energy costs. Apart from efficiency improvement, the power density of these converters has increased considerably and a smaller form factor is preferred by modern industrial plants. Power converters produce unwanted harmonics which deteriorate the grid current quality. To mitigate the adverse effects of such harmonics, filtering techniques such as active/passive filters and harmonic traps are employed. Passive inductors play an important role in these filtering topologies. However, in higher power/utility scale power conversion systems, due to lower switching frequency, the size and weight of passive inductor is large and they occupy considerable space. In industries such as offshore oil drilling and maritime transportation, size and weight requirements are strict and such bulky solutions are not desirable.

For such applications, an effective way to make passive components compact is to emulate using active devices. In this thesis, design of an Active Inductor for high power applications using an H-bridge topology is proposed. The performance of common filtering topologies such as LC and LCL with Active Inductor replacing a passive inductor is analyzed. The proposed topology emulates an inductance value which is linear for a wide range of operation, devoid of saturation issues and is compact in size and weight. Weight and volume analysis is done for an active topology and compared with equivalent passive inductors. It is shown that the emulated inductor is

about 8 times lighter than a passive inductor of similar rating. Also, loss analysis proves that the topology has a high Q factor. A Zero Voltage Switching (ZVS) switching method is proposed to reduce switching losses further.

In addition, the dynamic behavior of the Active Inductor improves system performance during faults and disturbances. The value of inductance can be tuned to suit the requirements of the overall power conditioning circuit. The Active Inductor is shown to limit the current and voltage overshoots occurring due to faults. Simulation and experimental results from a laboratory prototype confirm the validity and utility of the proposed topology.

ACKNOWLEDGEMENTS

I would like to express my gratitude to my advisor and committee chair, Dr. Enjeti, for his invaluable technical guidance and encouragement throughout my research. I would like to thank my committee members Dr. Balog, Dr. Bhattacharyya and Dr. Kim for their time and input.

Also, I would like to thank my fellow students, especially Bahaa, Pawan, Somasundaram, Harish and Puspa, working in the Power Electronics and Power Quality laboratory at Texas A&M University, for their time and patience.

Finally, I would like to thank my mother, father and sister for their constant encouragement throughout my graduate study.

TABLE OF CONTENTS

Page

Page

Page

LIST OF FIGURES

Page

Page

Page

Page

LIST OF TABLES

Page

1. INTRODUCTION

1.1 Importance of Adjustable Speed Drives (ASDs)

World energy consumption has increased considerably over the past few decades. Fossil fuel energy cost has increased and it still remains dominant in the energy basket as shown in Figure 1. Hence, industries have to contend with rising energy prices.

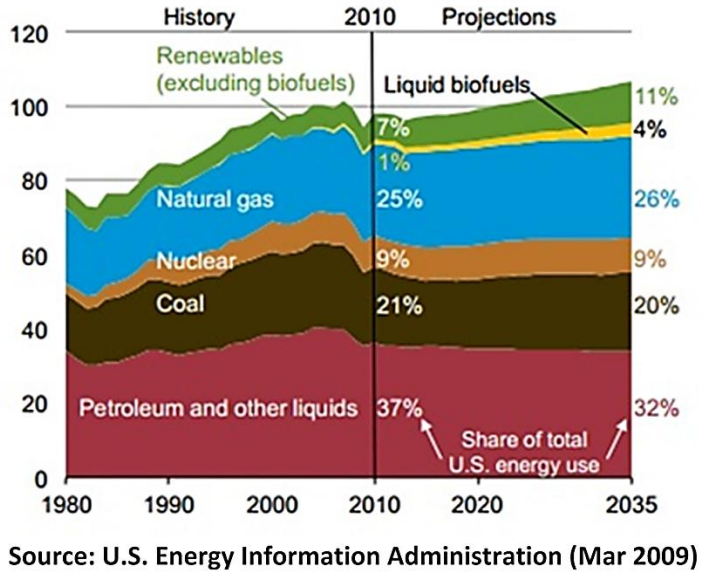

Figure 1: Primary energy use by fuel, 1980-2035 (quadrillion Btu). Reprinted with permission from [1]

The focus of industries across all sectors has been to increase efficiency. Motor driven systems are the workhorse of several industries and they consume roughly half of the world energy as shown in Figure 2. Hence, the industries have moved to ASDs over linear drives to increase the efficiency of motors. ASDs also bring additional benefits of improved durability, reliability and robust dynamic performance.

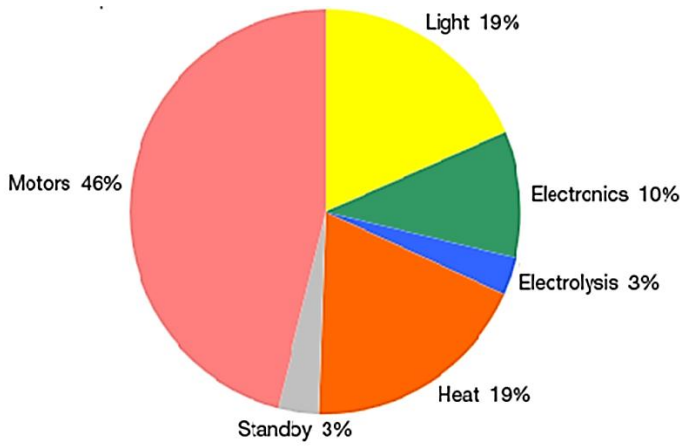

Energy Efficiency Policy Opportunities for Electric Motor-Driven Systems © OECD/IEA, 2011, source: A+B International (2009)

Figure 2: World energy consumption by percentage in 2006. Reprinted with permission from [2]

Thus, the world market for ASDs has reached $11.2 billion in 2011 and is expected to touch $16.3 billion by 2016 according to a report by IHS [3] as shown in Figure 3. Apart from efficiency improvement, it is desired by industries that the ASDs become lightweight and compact. Industries such as offshore drilling, shipboard and aircraft systems operate with a limited space infrastructure and cannot afford to have heavy and space occupying systems within the constraints they have to operate. Hence, it is extremely important for these industries to adopt latest technologies to reduce the size and weight requirements with little or no loss in efficiency.

1.2 Need for compact and lightweight systems

Consumer electronics over the years have become extremely lightweight and compact. Even in industry, lightweight systems which process more power per unit weight are becoming desired. For certain industries, the need for compact and

lightweight systems is much more because of the strict constraints. Every bit of saved space and reduced weight in the overall structures results in huge savings.

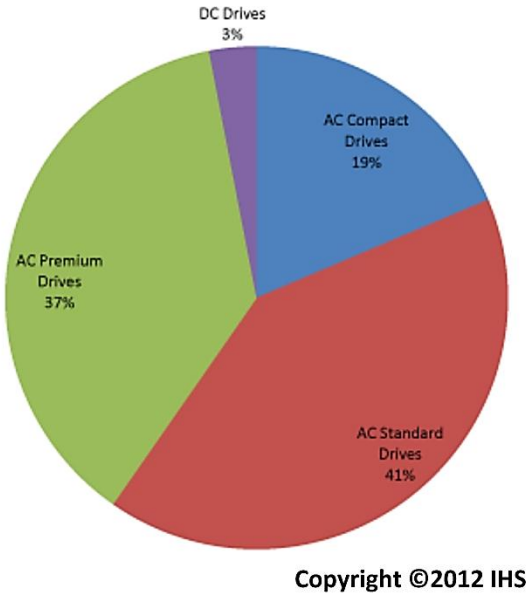

Figure 3: Motor drive market in the world as percentage, 2011. Reprinted with permission from [3]

Offshore drilling rigs are now built in deeper waters with depths of up to 7000ft and have to operate in severe conditions [4]. These rigs need subsea support structures which make the operation of all equipment safe and reliable. As a result, the equipment needs to be lightweight, for the subsea structure to provide stability. In order to increase the amount of petroleum production, it is desired to have more functionality within a limited space. For example, in [5] it has been shown that compact physical and chemical treatment technologies are preferred on the offshore rig. The subsea cables which go upto 6000 ft in some cases use special thin-wall jackets and insulation to save space and

reduce weight [6]. Hence, making the equipment smaller in size is also of extreme importance in order to optimize space usage.

Similarly, it is desired to have shipboard systems such as aircraft carriers and naval vessels to become as lightweight as possible and reduce the amount of energy spent in navigating with other heavy equipment. The cost of generating electricity at sea is higher than the cost of electricity produced at land [7]. Therefore, any reduction in weight is saving on cost of electricity. At the same time, such shipboard systems would like to have compact systems to house other major equipment.

There are similar constraints in aerospace systems as fuel expenses forms a major chunk of the cost of operation. Important equipment occupying less space in an aircraft or space shuttle will result in increased functionality within a limited space. A lot of efforts are being put to develop strong composites which will replace heavy materials as steel in aerospace applications and on offshore platforms for drilling [8]. Permanent magnet (PM) motors are lighter than induction motors and they are now a preferred solution in cruise vessel industry, oil and gas processing industry and are becoming popular in drilling and offshore wind turbines [9] . Table 1 shows the size advantages PM motors have over induction motors. These developments point to the fact that size and weight considerations are of utmost importance to these industries and every effort is being made to reduce size and weight of the overall system.

Table 1: PM motors vs induction motors. Reprinted with permission from [10]

Power Range (100-500HP)	Efficiency	HP/in^3	Hp/lb
PM motors	95-98%	0.15-0.2	1.5-1.7
Induction motors	90-93%	0.05-0.08	0.21-0.44

1.3 Need for compact ASDs

Offshore rigs and marine vessels employ several ASDs for powering up motors for various functions. As a result, the challenge for the designers is to reduce the size and weight of ASDs. In marine and shipboard military applications, size and weight are critical constraints in the design of shipboard power [7, 11]. In [7] the development of cost effective, lightweight ASDs is considered a big problem for naval applications. It details the cost gains to be made upon implementation of ASDs on shipboard systems. In [12], use of a medium frequency solid state transformer in a Medium voltage ASD is detailed in order to reduce size and weight of the overall system without compromising on the efficiency. With enhanced manufacturing capabilities, it is now possible to have several switches along with gating and protections integrated in one module and this helps to make ASDs even smaller and lighter [13]. Hence, designers and researchers are putting every effort to reduce the number of components and make the ASD system lightweight. With these efforts, since the 1980s the size of drives, measured in volume, has decreased by 70 to 80 percent, while the number of components has come down by 60 to 70 percent [14]. Manufacturers like ABB & Schlumberger now have specialized drives portfolio outlining their smaller footprint and light weight design to cater to these industries [15, 16].

1.4 Compact drives for renewable energy sources

A slew of large offshore wind generation farm projects are being planned across the world. Figure 4 shows the growing incidence of such farms. Delivering several hundred MW of power across the sea to the mainland grid will entail line losses.

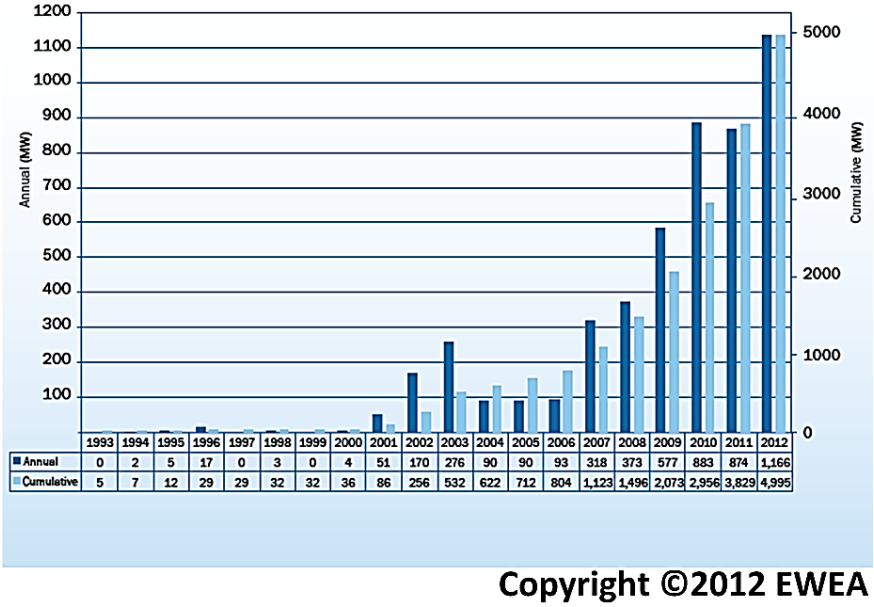

Figure 4: Energy production from offshore wind farms in Europe. Reprinted with permission from [17]

In such a scenario, it is important to keep the cost of generation low is important so that grid parity can be achieved. The converter substation requires a large structure to be built at sea involving huge costs. The foundation costs approximately between 15% and 40% of the total cost of current offshore wind farm projects [18]**.** The converter drive can be fitted within the body of the turbine if its size is significantly reduced. This will result in huge savings. In [19, 20] a new modular converter has been proposed that

can be integrated into a permanent magnet generator so that the overall system becomes lightweight and costs can be reduced.

Even for large scale photovoltaic (PV) projects, the number of projects has steadily increased as shown in Figure 5 as price of solar energy comes down. With a proliferation in these projects reliable and lightweight inverters are required to tie them to the grid. Usually for PV farms, a bulky line frequency transformer is necessary for galvanic isolation from grid. In order to solve this problem, smaller medium frequency transformers [22] and transformerless topologies [23] have been proposed. Therefore it is extremely important to focus on size and weight reduction of the ASDs which will be driving several high performance technologies operating in difficult conditions with size and space constraints.

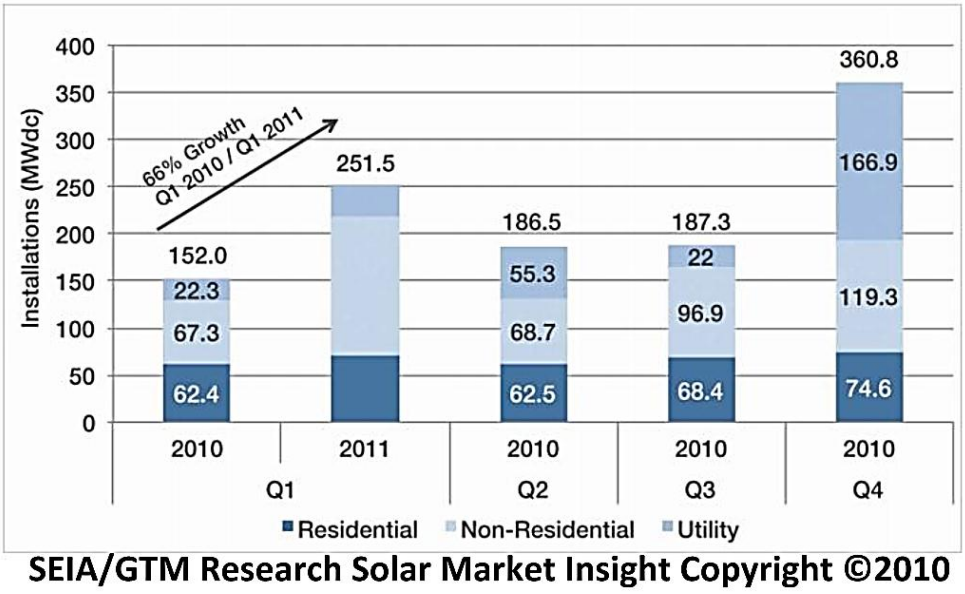

Figure 5: PV installations by segment in USA. Reprinted with permission from [21]

1.5 Research objective

The objective of this thesis is to propose and analyze an Active Inductor which will emulate a passive inductor suitable for high power applications such as offshore drilling and marine applications having weight and size constraints. The Direct Current (DC) link reactor in a diode rectifier fed ASD plays a major role in determining the grid current quality. A large DC-link reactor of 0.1-0.2 p.u. inductance improves grid current Total Harmonic Distortion (THD). However, it tends to be bulky for high power ratings, increasing the weight/volume. On the other hand, a smaller inductor (up to 0.01 p.u.) is of low volume, but makes the grid current quality poorer. The proposed Active Inductor can replace the DC link reactor in ASDs, improving the line current quality and mitigating the aforementioned weight and volume considerations.

In addition, it is dynamic in nature, changing the inductance value for improving system performance during grid faults. During grid faults, a PV farm inverter has to react quickly to prevent overcurrent tripping and component damage. An Active Inductor can emulate the grid side inductor in LCL filter of the inverter and increase the inductance value during the fault. Therefore, it can prevent overcurrent and increase reliability of the PV farm.

The concept of Active Inductor involves using an H-bridge topology, a capacitor as DC bus and a filter inductor. The controller emulates the desired inductance value by generating switching signals for the H-bridge to follow the voltage-current relationship of an inductor. The design methodology to select the components has been described. Simulation and experimental results are presented to prove the feasibility of the

proposed system. A prototype of the complete ASD system has been built in the laboratory and controlled using DSP.

An analysis is done to prove that the system response to grid faults and other step changes can be improved because of the dynamic nature of the inductor. A detailed size and weight analysis is done to find the actual benefits over an equivalent passive inductor for the DC link inductor in ASD system. The Active Inductor is shown to emulate a higher per unit inductance while having same size/weight as a low per unit inductance. A soft switching scheme to perform ZVS turn-on is investigated to reduce switching losses and improve Q-factor.

1.6 Thesis outline

The contents of the thesis are organized in the following manner. The introduction in Section 1 outlines the importance of compact and lightweight systems in industry. Power converters like ASDs have become popular because they increase efficiency and enhance reliability of systems. However, strict constraints on size and weight require constant innovation in drive technology to increase power density.

Section 2 discussed the significance of compact and lightweight design of power converters in industry especially in offshore drilling and marine industry with strict weight and volume constraints. A literature review is done to present the efforts which have made ASDs power dense over the years. The importance of passive components in power conditioning is explained along with their limitations they bring in design because

they are bulky. Various topologies which attempt to emulate passive components using active devices are also discussed along with their limitations.

The proposed Active Inductor concept was explored in section 3. The topology and the advantages were discussed in detail. A design methodology to choose the individual components was described. The control strategy to regulate the dc bus voltage of the inductor and implement inductive behavior was also explained. Small signal modeling of the proposed topology was done for an ASD and impact of parameter step response was assessed.

Section 4 presents the applications of the Active Inductor. Design strategy and simulation results of an ASD with a diode rectifier front end employing Active Inductor as the DC-link reactor has been shown. Experimental results from a scaled down prototype were also presented to validate the concept. A ZVS switching scheme to reduce the switching losses was also discussed. An LCL filter of a PV farm inverter with Active Inductor emulating the utility side inductor was also designed and simulated. The Active Inductor improves the performance of the inverter during LVRT.

Section 5 details a weight, volume and loss analysis of the Active Inductor emulating a DC link reactor in an ASD. Comparison has been done with corresponding passive inductor to portray the benefits. Loss analysis shows slightly increased losses in the Active Inductor which is still less than 1% of the rated power.

Section 6 provides the general conclusion of the work and discusses the scope and future work.

2. LITERATURE REVIEW

2.1 Importance of compact design of power converters

In 2003 a road mapping initiative was started by the European Center of Power Electronics (ECPE) to decide the future role of power electronics and to identify the technological constraints. Among these constraints, volume and weight of future power conditioning topologies were deemed important, as shown in Figure 6 [24].

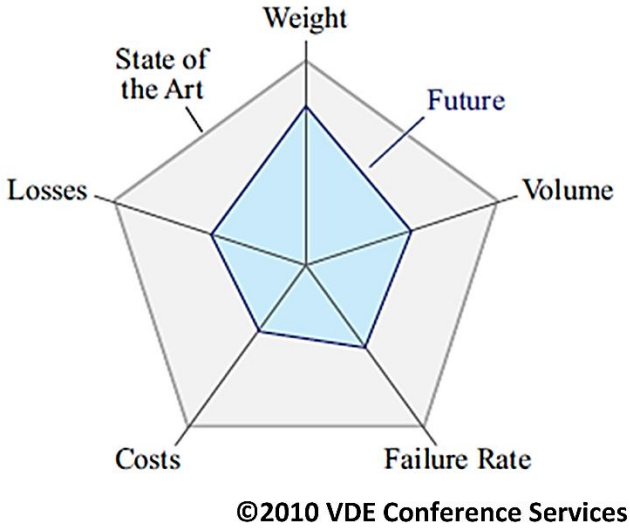

Figure 6: Required future performance improvement. Reprinted with permission from [24]

The power density of converters has roughly doubled every 10 years since 1970 because of increase in converter switching frequencies ten times every decade [25]. This increase in power density is of special importance to industries like the telecom industry as the space and weight requirements have become extremely strict. An attempt to

optimize efficiency and size/weight requirement for telecom power supplies has been made and several topologies have been analyzed to find the best solution [25]. Several other power conditioning topologies are required by industries having tight space and weight requirements.

2.1.1 Shrinking space and weight requirements

Several modern industrial plants have limited floor space and have design specifications for volume and weight of systems to be installed. Since 1980s the size of ASDs, measured in volume, has decreased by 70 to 80 percent, while the number of components has come down by 60 to 70 percent. The ASDs are now being designed to use a bookshelf design for industries which assign more importance to lower space requirement. These premium drives of 90 to 200 kW versions measure only 250 mm wide and 200–500 kW units only 350 mm wide. The compactness has been made possible by employing the latest technologies, such as new-generation switches and innovative cooling systems [14]. With the new roadmaps like the one by ECPE being implemented across the world, the size and weight of ASD systems are expected to reduce further.

With rapidly changing demands consumers, changing regulatory norms and a constant drive to better margins, industries have to constantly upgrade the plants using retrofits. A key factor for retrofits is space, as the area required for replacement units is generally not considered at the time of plant commissioning. Hence there is a huge market for ASDs which can improve capabilities and efficiency in retrofit and upgrade

projects [26]. In order to add these functionalities in the same space, the new ASDs are expected to be smaller.

Like the ECPE, the US Navy also has a technology roadmap which proposes a medium voltage DC system which will accommodate an increased power capacity using ship's limited available onboard space. Semiconductor devices with high voltage and high switching frequency capability are considered essential for a more compact power conditioning [27]. In [27], it has been shown that for medium voltage applications, Silicon Carbide (SiC) devices will be more suitable at high frequency operation which will reduce the size of energy storing passive elements like capacitors and inductors. They will have lower losses compared to Si devices shrinking the cooling requirements.

In [11] a distributed Energy architecture is proposed for shipboard power which reduces the size of the overall system and makes more power available without additional components. It also reduces size, weight and cost by arranging components more optimally. Instead of having a single converter which feeds Alternating Current (AC) power to the propulsion system and auxiliaries requiring high power transformers, the converter is split and a DC bus feeds the individual components.

Typical loads like Heating Ventilation and Air-Conditioning (HVAC) systems, fluorescent lighting circuits with conventional and electronic ballasts and servers employ switched mode type power electronic converters which draw excessive harmonic currents with third harmonic (180 Hz) component. With more loads becoming non-linear in nature, Active Power Filters (APFs) have now replaced capacitor banks to reduce harmonics. Apart from giving a much better harmonic filtering, APFs provide additional

benefits of smaller space requirement and reduced cost [28]. Several topologies of APFs have been developed which further reduce the size of the system [29, 30].

2.1.2 Compact ASDs

With reducing size of systems in general, there are several efforts being made to reduce the size of ASDs as well. In [12] two new medium-voltage ASD topologies with medium-frequency-link transformer isolation are introduced. AC-AC converters on the front end convert the line frequency to medium frequency which reduces the size of the isolating transformer used. It also improves the input power factor as input harmonics become of higher order and the input filter becomes smaller in size. A Variable-Frequency Drive (VFD) having a Current Source Rectifier (CSR) front-end and a Voltage Source Inverter (VSI) that increases power density and compatibility with a shipboard environment. A detailed power density comparison is done to prove that CSR front end topology occupies less space compared to a Voltage Source Rectifier (VSR) front end [31]. With enhanced manufacturing capabilities, it is now possible to have several switches along with gating, protections and heat sink integrated in one module and this helps to make ASDs even smaller and lightweight. For certain applications even the control module can be housed in the same module space leading to more compactness [13].

2.1.3 Power converters for renewable energy

In [19, 20], a solution is proposed to reduce the weight and size of a generator converter system in a wind turbine. Generally, when a 2 level converter is used, it imposes a limitation because of the switch voltage rating. This is followed by a step-up transformer to interface with the main grid. This system is too heavy and large to be placed in the wind turbine housing. The proposed multilevel modular structure allows switches of lower voltage rating to share high voltage output from the generator and convert it for grid connection. The modular converter feeds into a DC bus which carries the power to the land for conversion into usable AC form. This removes the requirement of transformer at the wind turbine. In [19] the modular multilevel converter is used to feed to a high voltage AC bus which eliminates the need of a step-up transformer on the wind-farm to grid side coupling. This solution is useful where space is more of a constraint on land where the grid is being fed.

In [22] a multilevel converter for a large PV farm has been proposed which uses medium frequency transformer isolation reducing the size/weight. Transformer-less PV inverters have been explored [32] in order to make the inverter more power dense and efficient by reducing transformer losses. Without isolation, there could be a large ground leakage current which the topology proposes to solve.

2.2 Need for compact design of passive components

Power conditioning topologies produce grid current harmonics which reduces the power factor. Several filtering topologies are used to filter out these harmonics. Several

active filters with series and parallel topologies have been presented in literature. In order to cancel double frequency ripple in the grid current emanating from a single phase PV inverter, a ripple port topology has been discussed [33, 34]. Several of these topologies use inductors to reduce grid current harmonics. For passive topologies, inductors are combined with capacitors as LC or LCL filters to improve overall power quality. However, for high power ratings, passive components tend to be bulky and increase the weight/volume and cost of power conditioning topologies. Moreover, the impedance value cannot be dynamically adjusted and is susceptible to temperature variation and tolerances in manufacturing. Power density of inductors can be increased by employing better materials and newer geometries, however, they add to cost and are also susceptible to changes in temperature and saturation [35]. Further, the component tolerance is particularly high. In order to make the design compact, there have been several efforts to emulate these passive components. The basic idea is to store energy in a dense form and then convert it to behave like a passive component.

2.2.1 Emulation as mechanical networks

Efforts have been made to emulate inductors and capacitors by using the analogy between mechanical and electrical networks in which force corresponds to current and velocity corresponds to voltage. On analyzing spring-mass-damper systems, it can be easily seen from Table 2 that they correspond to inductor-capacitor-resistor systems.

Table 2: Mechanical-Electrical equivalence

Mechanical Parameter	Electrical Parameter
Force	Current
Velocity	Voltage
Spring	Inductor
Damper	Resistor
Kinetic Energy	Electrical Energy
Potential Energy	Magnetic Energy

In [36] synthesis of such mechanical systems has been discussed. In [37] it has been shown that a mechanical setup called inerter plays the same role as an electrical capacitor. However, mechanical systems are considered to be too heavy to be practically used and the problem of emulating passive components to make them light and compact does not get solved.

2.2.2 Emulation using active devices

There are many topologies to emulate inductors using active devices, i.e. circuits which have the properties of a passive component but are built using only capacitors and active devices. The basic idea of all these topologies is to store energy in a passive element and control the switching to use the energy in a desired fashion to emulate the behavior of the reference element. A well-known configuration of such Active Inductors comprises of two transconductance amplifiers (OTA circuits) and one capacitor (gm-C circuit) [38]. In [38] an Active Inductor configuration using current controlled voltage sources was proposed in where the value of the inductance is controllable. However, the

application of this circuit is for low power applications. With advancement in semiconductor technology, it is possible to have active devices with greater power densities suitable for higher power applications [35]. Such active devices like Si and SiC based devices can be used to emulate a passive energy-storing component for high power applications with a high power density.

Another method to dynamically vary inductance is by using TCR (Thyristor Controlled Reactor) as shown in Figure 7, which is widely used in STATCOMs. The current in the reactor can be varied from maximum (thyristor valve closed) to zero (thyristor valve open) by changing firing angle. Hence, the effective inductance is varied [39]. However, this produces low frequency harmonics and the blocking of inductor current produces huge $\frac{di}{dt}$ in the system.

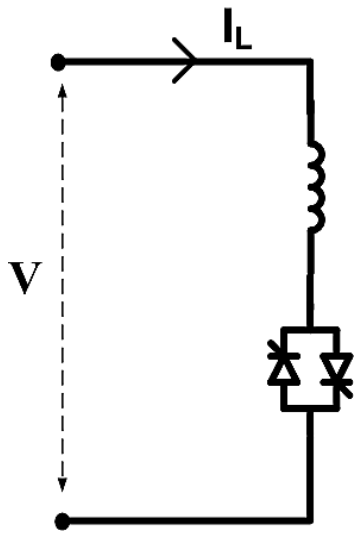

Figure 7: Thyristor controlled reactor

In [40] an active capacitor is proposed for capacitive coupling in Wireless Power Distribution, against the commonly used inductive coupling, to realize a higher power density. In [37], the idea of implementing such active capacitors to replace large buffer capacitive banks in a higher power systems, like STATCOMs is discussed. However, the discussion is limited to fundamental frequency and there is no detailed discussion on change in weight and size. In [41] a new topology with a half bridge and capacitor is shown to be used as an energy-storage buffer in the series-connected path with the line interface in a PV system. This buffer is designed to absorb the Power ripple at twice the line frequency. In [42] the concept of D-CAP (Dynamic capacitor) is presented which will absorb lower order harmonics or provide reactive VARs for a non-linear load. The topology is dynamic in nature and its parameters can be tuned to absorb harmonics of different orders. Figure 8 shows the D-CAP topology.

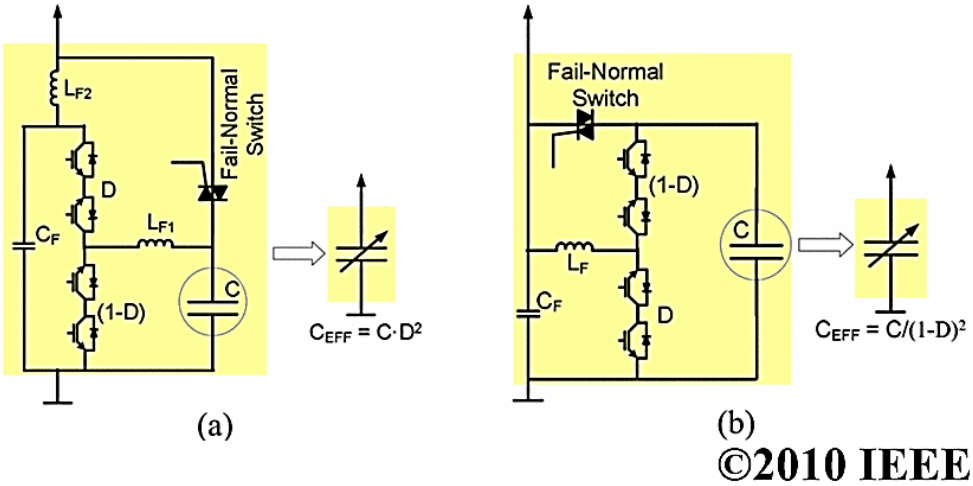

Figure 8: Proposed Dynamic Capacitor. Reprinted with permission from [42]

The topology is placed in parallel to the load and the duty ratio of the switches is modified in order to vary the amount of harmonic current or reactive VARs. However, placing the topology in parallel requires the switches to be rated for full voltage and this could be a prohibitive factor for high voltage systems.

Dr. Funato, in [43-45] has proposed the concept of variable active-passive reactance for high power applications. The basic modes of operation with the control algorithms involved are explained in detail.

The principle of operation of VAPAR for realization of inductor can be obtained from Figure 9.

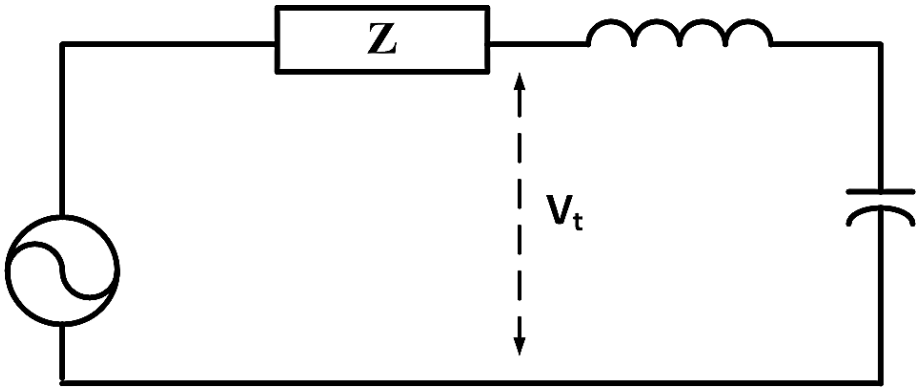

Figure 9: VAPAR model

The current reference I_{ref} is determined by integration of Active Inductor terminal voltage and dividing by reference inductance value, L_{ref}.

$$I_{ref} = \frac{1}{L_{ref}} \int V_t .dt \qquad (1)$$

Now using Laplace transform for solving the circuit by KCL and KVL:

$$V_x + V_c = \left(sL_{filter} + Z\right).I_t \tag{2}$$

$$V_c = K_p.\left(I_{ref} - I_t\right) \tag{3}$$

$$\mathrm{V_t} = V_x - Z.I_t \tag{4}$$

$$I_{ref} = \frac{1}{sL_{ref}}.V_t \tag{5}$$

Then the driving point impedance or the transfer function can be found after solving (2)-(5).

$$\frac{V_t}{I_t} = sL_{ref} \tag{6}$$

Hence, the inductive operation of the Active Inductor was proven. In [43, 45], several control topologies to achieve this operation are detailed. Methods like proportional control, hysteresis control and deadbeat control are a few of them.

One proposed application is power flow control by varying inductance. Power flow can be controlled by varying power angle between two buses carrying equal of different voltages as shown in (7). The angle is determined by the line inductance. As the Active Inductor can be tuned to any value, the line inductance can be changed and power transfer can be controlled.

$$P = \frac{V_s V_r}{X}\sin\delta \tag{7}$$

However there are many practical limitations to this application.

- The ripple of the envelope around the fundamental frequency in the line current of an Active Inductor is determined by (8).

$$V_{dcBus} = L_f \frac{\Delta I_{ripple} \cdot f_{switch}}{D} \quad (8)$$

Hence, the ripple depends on the switching speed and actual filter inductor used. With Si based switches, there is a limit to the switching speed for such high power applications as the losses would be high. Lower switching speed will translate into either of the following:

i) A huge high frequency ripple in the line current making the system bulkier with EMI filters.

ii) A big filter inductor negating any improvement in size and weight reduction.

- Since the topology is placed in series in comparison to an active filter being parallel needs the system to be rated for the full current. With an application like line inductance for power transfer, the Active Inductor output voltage should be rated for the maximum voltage of the involved voltage sources. In such a scenario, the capacitor and the switches have to be rated for peak to peak voltage of the line voltage. Moreover, capacitor has to be derated for handling transients and fault conditions. This increases the system size and weight.
- In [43] it is claimed that reactive elements like inductors are bulky and an Active Inductor would create the same effective resistance in a compact and light form. However, a high voltage and current rating will make the capacitor large and the heat sink has to become huge because of the switching

losses. Hence the overall system will become bulky and will not have a huge advantage over the large and heavy inductor.

Given the limitations, an Active Inductor has to be chosen for the right application, having the following.

i) Stringent weight and space constraints.

ii) No significant losses maintaining similar overall system efficiency.

iii) Limited voltage or current rating compared to the overall system.

2.3 Conclusion

The importance of reducing the size and weight of power conditioning topologies has been discussed in the section. The need of industry to consistently increase power density of power conditioning topologies is highlighted. The strict constraints that certain industries have to face have also been emphasized. Inductors play an important role in power conversion and it is important for these industries to reduce the weight/size of inductors. Efforts which have been made to emulate the inductor have been detailed. The VAPAR was proposed to emulate an inductor for power transmission application. The benefits and limitations of the topology have been listed.

3. PROPOSED ACTIVE INDUCTOR TOPOLOGY & CONTROL STRATEGY

3.1 Introduction

The Active Inductor topology employs the energy stored in a capacitor and converts it to inductive form using the switching strategy. The design of the Active Inductor topology is shown in Figure 10. The structure can be broadly divided into two main sub-systems, power converter and DC link capacitor for energy storage.

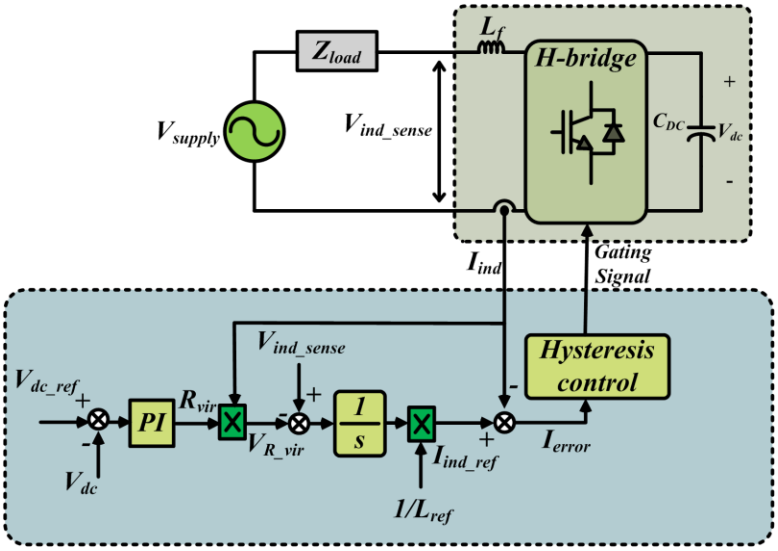

Figure 10: Proposed Active Inductor topology with control system

The proposed topology has the following advantages

- The proposed Active Inductor results in compact construction, small footprint and lightweight design. It gives more flexibility to system designers and

makes more space available for other needs particularly in specialized applications where weight and space constraints are stringent.

- The inductance value can be adjusted for different utility impedance per installation. The inductance value can also change dynamically during fault conditions or when the input voltage becomes heavily distorted.
- The filter inductor used is much lower in inductance value. Hence, derating the inductor for maximum flux density increases the size of the overall system by a small value.
- The Q factor of the Active Inductor can be designed to be high by using new semiconductor technologies like SiC and GaN devices and employing advanced switching schemes with ZVS [46].
- The proposed Active Inductor is envisioned to be a direct plug and play replacement of passive components in many retrofit applications, saving considerable cabinet space and improve performance.

3.2 Proposed Active Inductor topology

The power converter chosen for this application has to meet several requirements. It needs to operate at a high switching speed without adding to losses significantly. It has to withstand high temperatures while exhibiting fault tolerant behavior and failsafe mode in order to maintain system availability. It needs to keep the capacitor charged to the desired value. At the same time, it needs to convert the energy

for the system to emulate inductive behavior. The right choice for the power converter is an H-bridge topology which can obtain three level output according to Table 3.

Table 3: 3 state operation

State	Switches ON	Switches OFF
1	SW1 & SW4	SW2 & SW3
0	None	All
-1	SW2 & SW3	SW1 & SW4

The switching pattern can then be selected to charge and discharge the DC Link capacitor and also make the system behave as an inductor as it can attain both positive and negative voltage across its terminals.

3.2.1 H-bridge

For higher switching speed with lower losses and smaller heat sink requirement, SiC devices can be selected. In [47] an analysis of a high power half bridge SiC Metal-Oxide-Semiconductor Field Effect Transistor (MOSFET) module is detailed and compared with Si IGBT Module. It is shown that at high frequency operation, the losses are significantly lower. At the same time, the temperature rise is also lower. This makes SiC MOSFETs a good choice for the H-Bridge. GaN devices can also be used for lower voltage applications.

3.2.2 Energy storage

The DC link capacitor stores the energy required to emulate the inductance. It should also withstand high RMS currents have low capacitance drift at high temperatures and frequency. The capacitor could be selected as a metalized polypropylene film capacitor to fulfill the requirements above for increased reliability as shown in Figure 11.

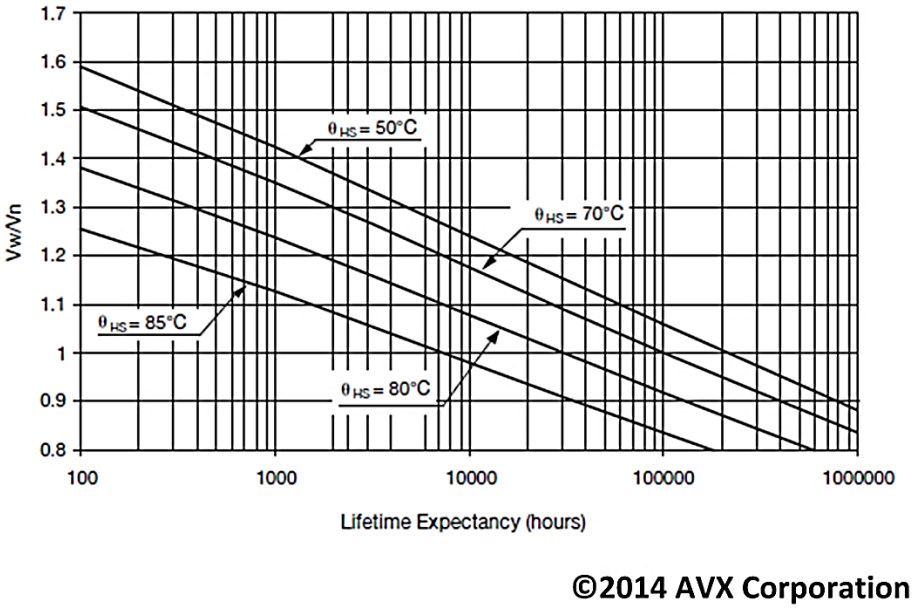

Figure 11: Film capacitor reliability: Life expectancy vs operating voltage and operating temperature. Reprinted with permission from [48]

3.2.3 Filter inductor

A small high frequency inductor, L_f will be required for power transfer and filtering out current harmonics. The inductor has to be made of a material which has low losses at high frequency operation. Traditionally for low frequency operation, silicon

steel is the preferred material. However, for high frequency operation in DC-DC converters like boost converter and flyback converter, ferrite core is preferred. One limitation of the ferrite core is the saturation flux density of 0.38T which will increase the size drastically. Recent developments in core material have increased the number of choices for high frequency core material. Nanocrystalline material has excellent core properties owing to high flux density and low losses at high frequencies. Hence, an ideal choice for the filter inductor core could be a Nanocrystalline core [49].

One common problem encountered by magnetics designers is the saturation of inductors. To overcome this problem, usually the design maximum flux density is kept much lower than the actual saturation flux density. This leads to a much larger inductor design adding further to space requirement and weight. The proposed Active Inductor uses a filter inductor which is much smaller than the value of actual emulated inductor. Hence, even derating for the saturation flux density increases the weight and size by a small value. The proposed topology is capable of carrying large value of DC current without saturation, exhibit linearity over a wide range without magnetic hysteresis and can be designed to operate at higher temperatures

3.3 Control strategy

The block diagram for the control of the proposed Active Inductor is shown in Figure 12. The controller structure consists of two loops. The inner loop is a current controller, while the outer loop is used to regulate the DC link voltage by employing a PI controller.

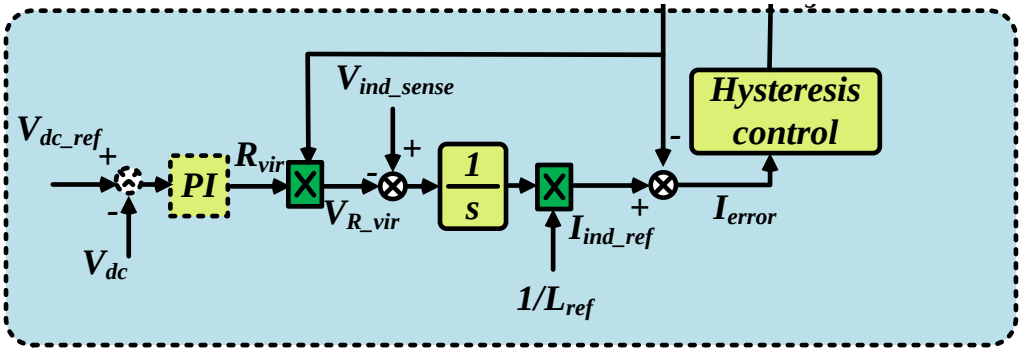

Figure 12: Controller for the proposed topology

3.3.1 Outer DC bus voltage control

An ideal Active Inductor system will have the voltage at its terminals and current 90° out of phase and will not be dissipating any real power. The DC-link capacitor would not need any voltage control as the average real power required by the system is zero as shown in Figure 13.

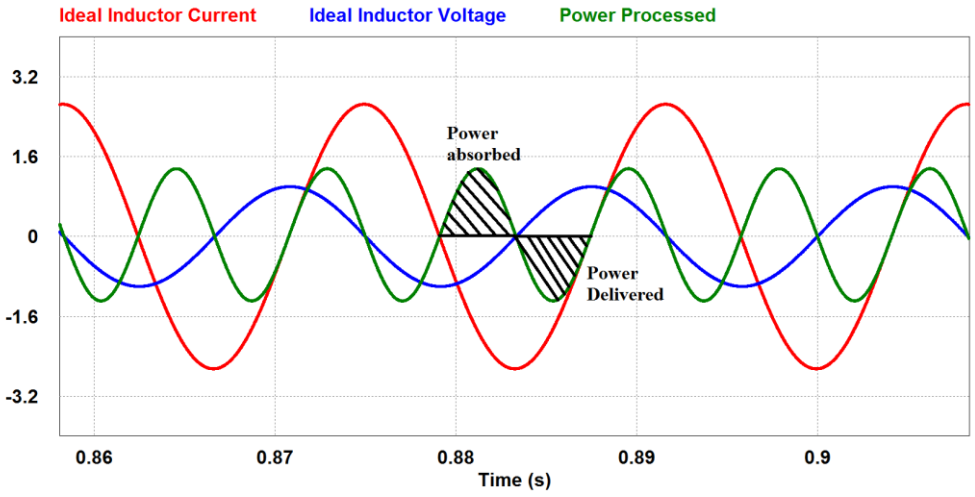

Figure 13: Power processed by an ideal lossless inductor

However, the system components have their losses and this would dissipate some real power. In order to compensate for this loss, the system needs real power to maintain constant DC link voltage, V_{dc} across the DC Link capacitor during regular operation. However, like an inductor the current and voltage should be in quadrature. Hence, the current and voltage will be slightly less than quadrature and a small amount of real power will flow into the system charging up the capacitor. The error between V_{dc_ref} & V_{dc} is passed through a PI block transfer function. This is represented by series virtual resistance with the desired inductance, R_{vir}. The idea behind the virtual resistance is to assume the system as shown in Figure 14 and estimate the equivalent resistance for all the losses in the system.

Figure 14: Real inductor with equivalent losses

The equivalent resistance of the system can be calculated from (9).

$$P_{loss} = I^2 R_{equivalent} \tag{9}$$

The PI controller produces the equivalent resistance, R_{vir} as output. The voltage drop across this virtual resistor, V_{Rvir}, is generated by multiplying the R_{vir} with inductor current, I_{ind}. This voltage drop is subtracted from the sensed inductor voltage, V_{ind_sense},

to generate the small deviation from quadrature between current and voltage. The created phase difference as shown in Figure 15 generates the required real power and compensates for the DC link voltage fluctuations. As a result, the PI controller regulates the DC link voltage close to the reference value, V_{dc_ref} .

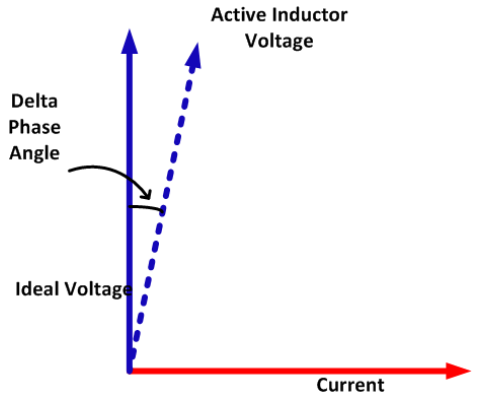

Figure 15: Phase angle deviation to maintain DC link voltage

3.3.2 Inner current control

The inner current loop calculates the commanded value of inductor current, I_{ind_ref} , by using the relationship between the sensed inductor voltage, V_{ind_sense} and I_{ind_ref} as in (10). The sensed current value, I_{ind} is subtracted from the reference value, I_{ind_ref} , and the resultant current error, I_{error} is fed to a current controller to generate the H-bridge gating signals. Hence the current control forces the H-bridge to draw mostly reactive power with some active power determined by the outer voltage control loop.

$$I_{ind\_ref} = \frac{1}{L}\int\left(V_{ind\_sense} - V_{R\_vir}\right)dt \qquad (10)$$

The current controller can be selected to be either a hysteresis controller or a proportional controller.

3.3.2.1 Hysteresis control

A virtual envelope, as shown in Figure 16 is created around the reference current command and the inductor current is forced to remain within the envelope. The boundaries of the envelope could be selected as 5% or 10% of the actual current which results in good regulation. Figure 17 shows experimental results demonstrating the same effect.

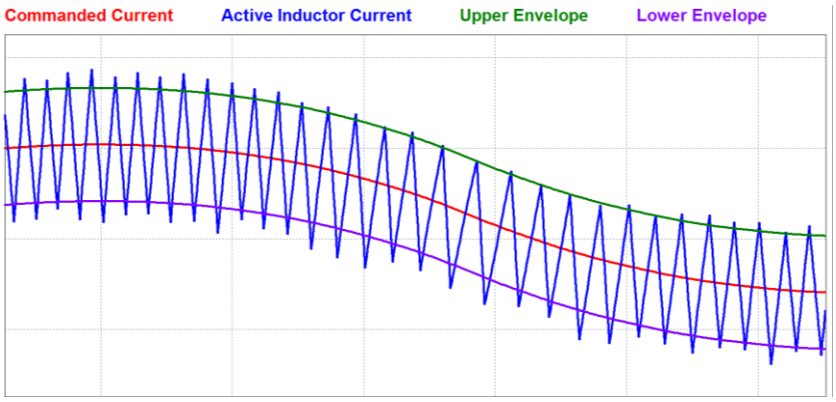

Figure 16: Hysteresis control: Active Inductor current bounded by envelope

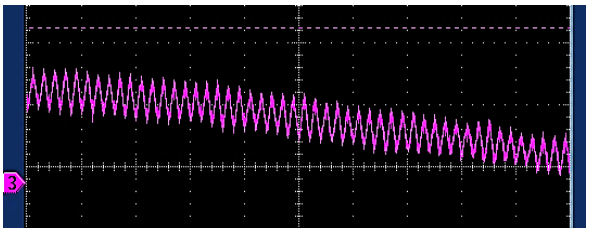

Figure 17: Hysteresis loop performance in experimental result

$SW_1 \& SW_4 : I_{ind}$ > Upper Envelope

$SW_2 \& SW_3 : I_{ind}$ < Lower Envelope

However, in this method, the frequency of switching fluctuates. For many applications this is not suitable as they would not like operation at certain frequencies. Moreover an EMI filter targeted at a particular frequency cannot be designed. A variable frequency leads to an unpredictable loss profile and requires highly derated heat sink design.

3.3.2.2 Proportional control

A fixed frequency triangular waveform is used as a carrier signal and the current error multiplied by proportional value is used as the control waveform.

$SW_1 \& SW_4 : V_{control} > V_{tri}$

$SW_2 \& SW_3 : -V_{control} > V_{tri}$

Here the regulation depends on the switching speed selected as shown in (11).

$$V_{dcBus} = L_f \frac{\Delta I_{ripple} \cdot f_{switch}}{D} \quad (11)$$

Now assuming, V_{dcBus} is regulated at a constant value, ΔI_{ripple} will depend on the switching speed and duty ratio. In case there are fluctuations in V_{dcBus}, the ripple in current will increase unlike Hysteresis controller. Hence the regulation is less tight. However, the switching is constant and this allows us to make precise choice of switching speed which does not interfere with frequencies of other systems nearby. A

targeted EMI filter can be designed and the heat sink design is also simpler as loss analysis can be done easily.

3.4 Small signal modeling & analysis

A small signal analysis of the topology is done to find relevant transfer functions of the system in open loop and closed loop. Figure18 shows the small signal model used for the purpose.

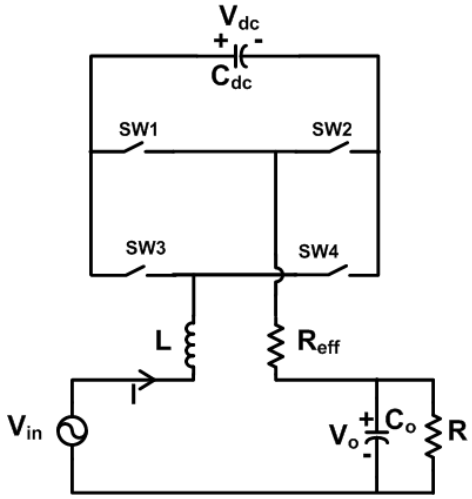

Figure 18: Small signal model of Active Inductor

The state space model of the model is derived by assuming 2 states. In state 1 SW2 and SW3 are closed as shown in Figure 19.

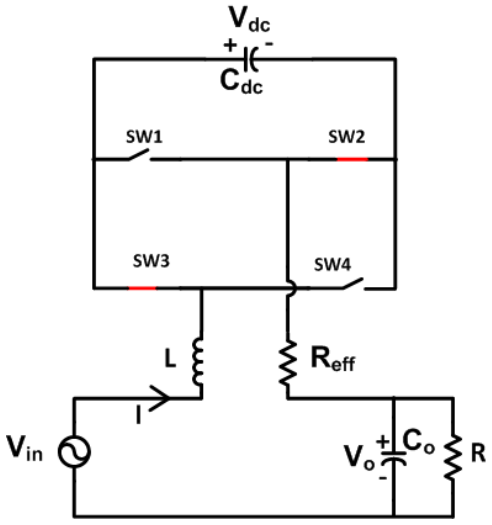

Figure 19: State 1 of small signal model

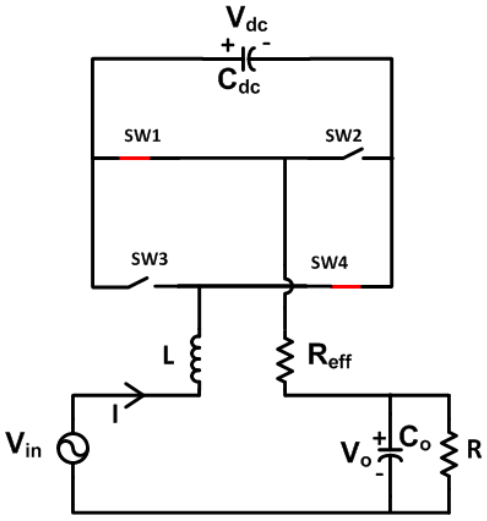

Figure 20: State 2 of small signal model

In state 2 SW1 and SW4 are closed as shown in Figure 20.

The state space model is given by:

$$\begin{bmatrix} \overset{*}{i} \\ v_{dc} \\ v_0 \end{bmatrix} = A \begin{bmatrix} i \\ v_{dc} \\ v_0 \end{bmatrix} + Bv_{in} \tag{12}$$

$$i = C \begin{bmatrix} i \\ v_{dc} \\ v_0 \end{bmatrix} \tag{13}$$

State 1 matrix:

$$A_1 = \begin{bmatrix} -\frac{R_{eff}}{L} & \frac{-1}{L} & \frac{-1}{L} \\ \frac{1}{C_{dc}} & 0 & 0 \\ \frac{1}{C_o} & 0 & \frac{-1}{RC_o} \end{bmatrix};\ B_1 = \begin{bmatrix} \frac{1}{L} \\ 0 \\ 0 \end{bmatrix};\ C_1 = [100] \tag{14}$$

State 2 matrix:

$$A_2 = \begin{bmatrix} -\frac{R_{eff}}{L} & \frac{1}{L} & \frac{-1}{L} \\ \frac{-1}{C_{dc}} & 0 & 0 \\ \frac{1}{C_o} & 0 & \frac{-1}{RC_o} \end{bmatrix};\ B_2 = \begin{bmatrix} \frac{1}{L} \\ 0 \\ 0 \end{bmatrix};\ C_2 = [100] \tag{15}$$

Equivalently, $A = A_1 D + A_2 D'$, $B = B_1 D + B_2 D'$, and $C = C_1 D + C_2 D'$

$$A = \begin{bmatrix} -\frac{R_{eff}}{L} & \frac{1-2D}{L} & \frac{-1}{L} \\ \frac{2D-1}{C_{dc}} & 0 & 0 \\ \frac{1}{C_o} & - & \frac{-1}{RC_o} \end{bmatrix};\ B = \begin{bmatrix} \frac{1}{L} \\ 0 \\ 0 \end{bmatrix};\ C = [100] \tag{16}$$

In order to find the small signal model transfer functions, perturbations from steady state for all parameters are considered.

Small signal model:

$$\hat{\dot{x}} = A\hat{x} + [A_1 - A_2]x_o \hat{d} \tag{17}$$

$$\hat{y} = C\hat{x} \tag{18}$$

where,

$\hat{d}$ is perturbation in duty ratio,

x_o is steady state matrix

$$A_1 - A_2 = \begin{bmatrix} 0 & \frac{-2}{L} & 0 \\ \frac{2}{C_{dc}} & 0 & 0 \\ 0 & 0 & 0 \end{bmatrix} \tag{19}$$

Transfer function of line current to duty ratio:

$$\frac{\hat{i}}{\hat{d}} = C[sI - A]^{-1}[A_1 - A_2]\begin{bmatrix} I \\ V_{dc} \\ V_o \end{bmatrix}, \text{ where } C = [100] \tag{20}$$

In steady state current can be assumed to be DC and duty ratio D can be assumed to be 0.5. Solving (20) we get (21).

$$\frac{\hat{i}}{\hat{d}} = \frac{-2\frac{V_{dc}}{L}.\left(s + \frac{1}{RC_o}\right)}{s^2 + \frac{\left(L + RC_oR_{eff}\right)}{LRC_o}s + \frac{R + R_{eff}}{RLC_o}} \tag{21}$$

Transfer function of output voltage to duty ratio:

$$\frac{\hat{v}_o}{\hat{d}} = C[sI - A]^{-1}[A_1 - A_2]\begin{bmatrix} I \\ V_{dc} \\ V_o \end{bmatrix}, \text{ where } C = [001] \tag{22}$$

$$\Rightarrow \frac{\hat{v}_o}{\hat{d}} = \frac{-2\frac{V_{dc}}{LC_o}.}{s^2 + \frac{\left(L + RC_oR_{eff}\right)}{LRC_o}s + \frac{R + R_{eff}}{RLC_o}} \tag{23}$$

Transfer function of current to input voltage:

$$\frac{\hat{i}}{\hat{v}_{in}} = C[sI - A]^{-1}B, \text{ where } C = [100] \tag{24}$$

$$\Rightarrow \frac{\hat{i}}{\hat{v}_{in}} = \frac{\frac{1}{L}.\left(s + \frac{1}{RC_o}\right)}{s^2 + \frac{\left(L + RC_oR_{eff}\right)}{LRC_o}s + \frac{R + R_{eff}}{RLC_o}} \tag{25}$$

Transfer function of current to commanded inductance, L_{ref} can be found out after considering the flow diagram shown in Figure 21.

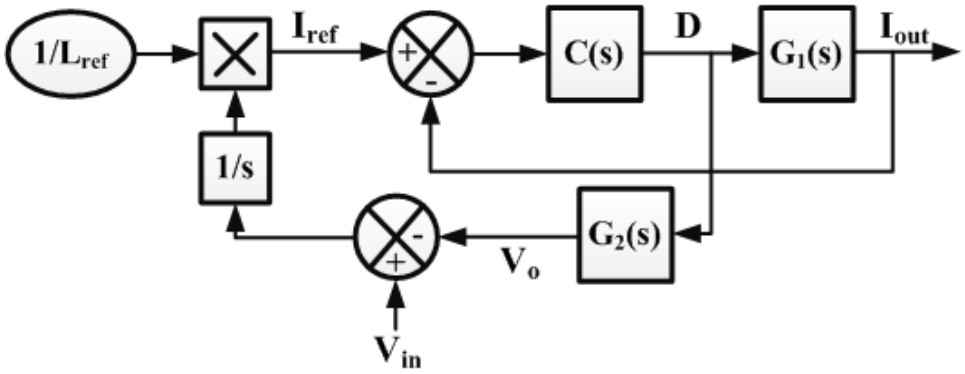

Figure 21: Control block diagram

where

$$G_1(s) = \frac{\hat{i}}{\hat{d}} = \frac{-2\frac{V_{dc}}{L}.\left(s + \frac{1}{RC_o}\right)}{s^2 + \frac{\left(L + RC_oR_{eff}\right)}{LRC_o}s + \frac{R + R_{eff}}{RLC_o}};$$

$$G_2(s) = \frac{\hat{v}_o}{\hat{d}} = \frac{-2\frac{V_{dc}}{LC_o}.}{s^2 + \frac{\left(L + RC_oR_{eff}\right)}{LRC_o}s + \frac{R + R_{eff}}{RLC_o}};$$

C(s) is control block.

Solving for Figure 21, the transfer function of current to commanded inductance, L_{ref} is given by

$$\frac{i}{1/L_{ref}} = \frac{\frac{1}{s}\left(V_{in} - DG_2(s)\right)}{1 + \frac{1}{CG_1(s)}} \tag{26}$$

assuming,

$$m = \frac{\left(L + RC_o R_{eff}\right)}{LRC_o}; n = \frac{R + R_{eff}}{RLC_o}; l = \frac{1}{RC_o}; B = \frac{-2V_{dc}C(s)}{L}$$

$$\frac{i}{1/L_{ref}} = \frac{\frac{B}{s}\left[s^3(V_{in}+1) + s^2\left(2m+l\right) + s(ml + 2n + 4dV_{dc}) + \ln + 2dlV_{dc}\right]}{s^4 + 2s^3(B+m) + s^2(2mB + lB + m^2 + 2n) + s(mlB + 2nB + 2mn) + B\ln + n^2} \tag{27}$$

3.4.1 Voltage step change response

Transfer function for current to input voltage can be found from (25). The steady state can be found by putting s=0.

$$\frac{I}{V_{in}} = \frac{1}{R + R_{eff}} \tag{28}$$

For transient response, we consider a system with values as shown in Figure 22.

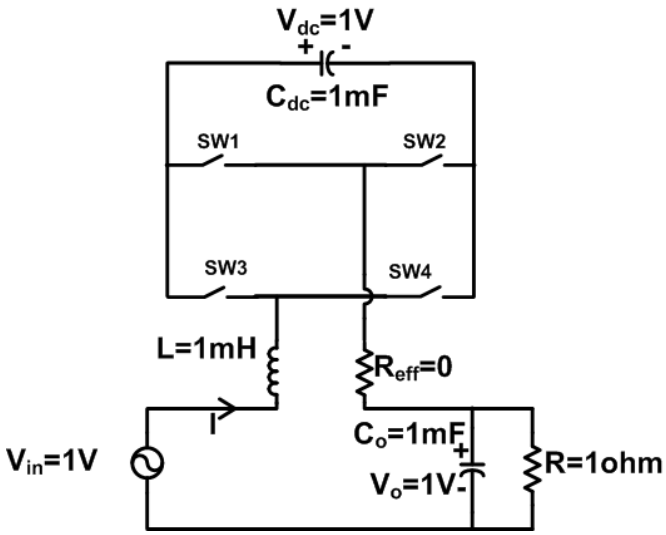

Figure 22: Simplified model for small signal analysis

$$\frac{\hat{i}}{\hat{v}_{in}} = \frac{10^3.\left(s+10^3\right)}{s^2+10^3 s+10^6} \tag{29}$$

$$Poles = -500 \pm 866\,j$$

$$Zeroes = -1000$$

Both the poles and zero on left hand side. Hence the system is stable.

3.4.2 Load step change response

In order to analyze a load step change to the system, transfer function of current to duty ratio in (21) is considered and load is selected as a variable as shown in (30).

$$\frac{\hat{i}}{\hat{d}} = \frac{-2000.\left(s+\frac{10^3}{R}\right)}{s^2+\frac{10^3}{R}s+10^6} \tag{30}$$

$$Poles = \frac{-500}{R} \pm \frac{500}{R}\sqrt{1-4R^2}$$

$$Zero = \frac{-1000}{R}$$

For any real value of R, zero will always be on left hand side. For an RHP, $\sqrt{1-4R^2} > 1$ which will never be true. Hence both poles are LHP making the system stable for any value of R.

3.4.3 Reference inductance step change

To consider the impact of step change in L_{ref} we need to solve (27) for the given circuit in Figure 21. Assuming proportional controller, $C(s) = K_p$.

$$m = 10^3; n = 10^6; l = 10^3; B = -2000K_p$$

$$\frac{i}{1/L_{ref}} = \frac{\frac{-2000K_p}{s}\left[2s^3 + 3.10^3 s^2 + 3.10^6 s + 10^9 + 2.10^3 d\right]}{s^4 + 10^3.s^3(2-4K_p) + 10^6 s^2(3-6.K_p) + 10^9 s(2-6K_p) + 10^{12}.(1-2K_p)} \quad (31)$$

By varying K_p the pole-zero plot can be obtained to find stable roots. Figure 23 shows the pole-zero plot with K_p being varied from 0.001 to 0.25. 'x' marks the poles while 'o' marks zeroes. Zeroes stay same as Duty ratio, d = 0.5. Poles start moving towards RH of plot as the K_p is increased. Beyond K_p = 0.25 the poles are at RHP. In addition there is always a pole at zero which is not considered in the plot. This pole makes the system slow yet stable.

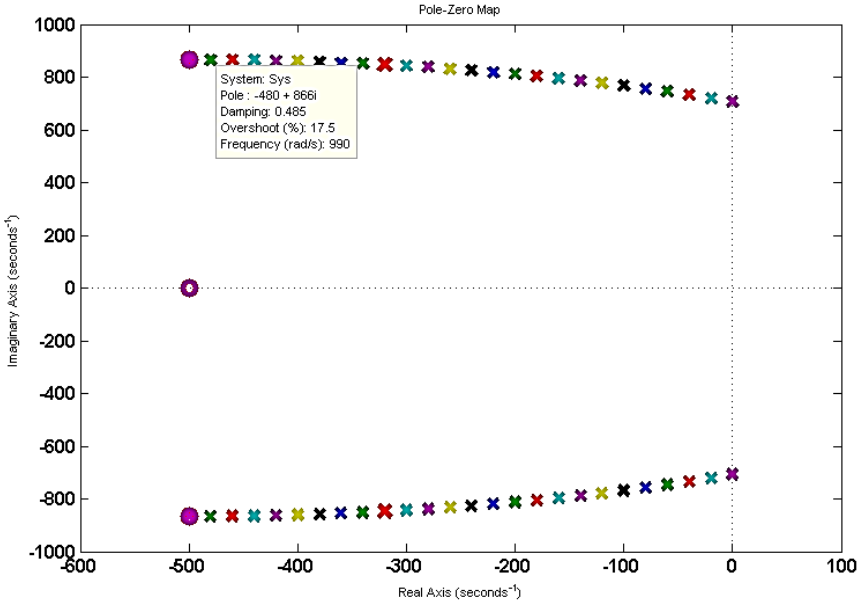

Figure 23: Pole-zero plot for current to L_{ref} transfer function with varying K_p.

3.5 Conclusion

The proposed concept of Active Inductor has been explained along with its essential components. An H-bridge topology is selected for meeting all the requirements of the topology of charging the capacitor and switching to generate an inductive behavior. Design of capacitor and filter is also discussed. Control strategy for the Active Inductor is shown. Small signal modeling of the system is done to analyze step response in open loop and closed loop. Controller design methodology is also presented using results from the small signal modeling.

4. INDUSTRIAL APPLICATIONS FOR THE ACTIVE INDUCTOR

4.1 Introduction

The proposed topology aims to reduce the weight and size of the inductor. Hence, the Active Inductor will be of special interest to industries where making systems lightweight and smaller is of paramount importance. Several industries like offshore drilling and shipboard systems put a premium on these requirements. Power conversion for ASDs usually uses inductors as LC or LCL filters which are bulky. Two examples of the application of Active Inductor, one in an LC filter and another one in an LCL filter are discussed. The added benefits of using a tunable inductor in such systems are also explained.

4.2 Active Inductor to replace the DC link reactor in ASD system

Commercial ASD systems find widespread application in industry and mostly consist of diode bridge rectifier (6 pulse or 12 pulse) resulting in low frequency harmonics [50, 51]. In order to reduce the impact of these harmonics, ASD systems typically employ an LC filter to provide a smooth DC voltage and reduce AC line current harmonics. The LC filter constitutes of a bulk capacitor and a large DC link reactor which is generally designed for 0.05-0.1 p.u. of line impedance. Hence, this reactor is bulky and it contributes to increase in weight, volume and cost of the overall system. However, in many high performance applications like shipboard, aircraft systems and drilling, size constraints do not allow a large inductance value [26].

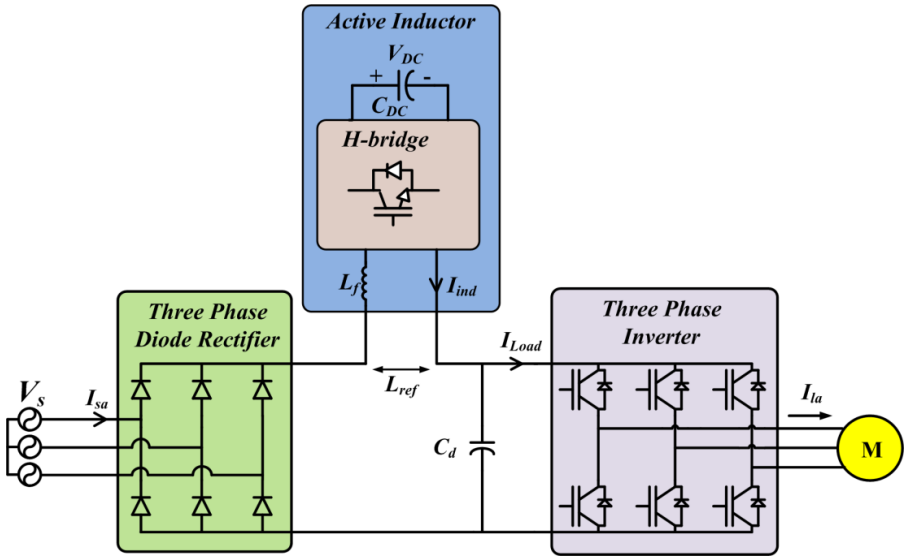

Figure 24: ASD with Active Inductor as DC-link reactor provides increased power density

The proposed Active Inductor replaces this bulky inductor as shown in Figure 24. As the Active Inductor is tunable, a commanded value of 0.1 p.u. can be selected. This provides a similar quality of load voltage, V_{load}, and a lower ripple on the inductor current, I_{ind}. Moreover, it has lower size/weight as the passive components used are of smaller size than the reference inductance value, L_{ref}.

4.2.1 Advantages over a Pulse Width Modulated (PWM) rectifier fed ASD system

In order to use a small inductor, a PWM rectifier may be used in the front end instead of a diode rectifier as shown in Figure 25. Such a system can use a small LC filter as the harmonics are of higher order.

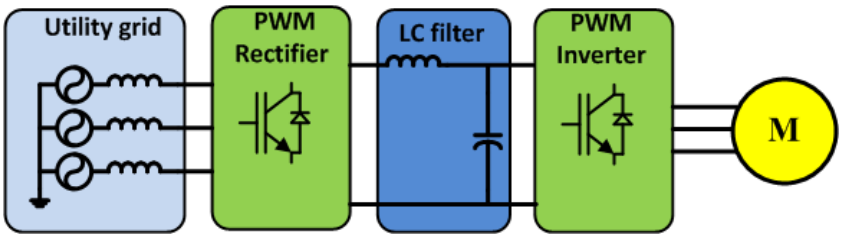

Figure 25: ASD with PWM rectifier as front end

Also, the inductor can be altogether done away with and have only the DC link capacitor. Such a configuration is also regenerative, although most motors do not need a regenerative ASD. However, this system has several disadvantages when compared to the configuration with Active Inductor.

- The PWM rectifier will be fully rated (1 p.u.) and will use 6 switches with voltage and current rating same as the ASD ratings. In comparison, the Active Inductor configuration will need 4 switches with lower voltage rating. This will reduce the costs further.
- The PWM rectifier fed ASD system will use three AC line reactors for power transfer which will increase the weight of the system.
- PWM rectifier will be more expensive than a diode rectifier.

4.2.2 System response in faults and distortions

As Point of Common Coupling (PCC) load distortion increases because of other non-linear loads, the voltage at the utility side on the rectifier input becomes distorted. If the filter designed for the ASD is not sufficiently attenuating the harmonics, voltage and current quality fed to the load by the ASD will reduce. For such a scenario, the filter

design has to be done for harmonic content much larger than the present specifications, which will increase the size and weight of the system. However, in similar conditions, the inductance of the Active Inductor can be increased and a high quality of voltage and current can be maintained. In case of a grid fault, the harmonics introduced by the utility and the UPS backup can also be smoothened by increasing the inductance value.

4.2.3 Design example: ASD system

The electrical specifications of the ASD for which the Active Inductor is to be designed are as shown in Table 4.

Table 4: ASD specifications for the proposed design

ASD Specifications	Rating
Input voltage, $V_{in,LL,rms}$	2.3 kV
Output power, P_{out}	1 MW
DC load current, I_{load}	330 A
Active Inductor, L_{ref} (0.1p.u.)	2.5 mH
Passive inductor, L_{pas} (0.01p.u.),	250 µH
Filter inductor, L_f (0.006p.u.)	150 µH
Active Inductor DC bus capacitor, C_{dc}	1.5 mF

Figure 24 shows the proposed ASD topology for 1 MW drive with Active Inductor replacing the DC link inductor. The line-to-line rms voltage $V_{in,LL,rms}$ is 2.3 kV which yields a DC bus voltage, V_{dcLink} of 3100 V. The three phase inverter converts V_{load} to three phase voltage using PWM switching at 6 KHz and supplies to an inductive

motor load of power factor, 0.75. For a three phase diode rectifier system, the THD for line current is lower for continuous conduction. However, for continuous conduction, a large DC link inductor is required. The minimum inductance value for continuous conduction is given by (32) [52].

$$L_{\min} = \frac{0.0129.V_{in,LL,rms}}{\omega.I_{load}} \tag{32}$$

The capacitance in the LC filter can be calculated by (33).

$$C_{dc-link} = \frac{I_{d,6}}{6.\omega.V_{load}.RF} \tag{33}$$

where $I_{d,6}$ is 6th harmonic component in the DC current; RF is the ripple factor on the DC link voltage.

For this system, the minimum DC link inductance is found to be $L_{\min}$ = 250 uH. $C_{dc-link}$ was found to be 1.5 mF. The inductance value can be described in terms of per unit line impedance. The line impedance is calculated from following (34).

$$Z_{line} = \frac{V_{dcLink}^{2}}{P_{out}} \tag{34}$$

The line impedance is found to be $Z_{line} = 9.61\ \Omega$. The per unit value of the DC link inductance can be found from (35) to be 0.01.

$$P.U. = \frac{\omega L_{choke}}{Z_{line}} \tag{35}$$

Figure 26 shows the line current THD as a function of Load Current, I_{load}.

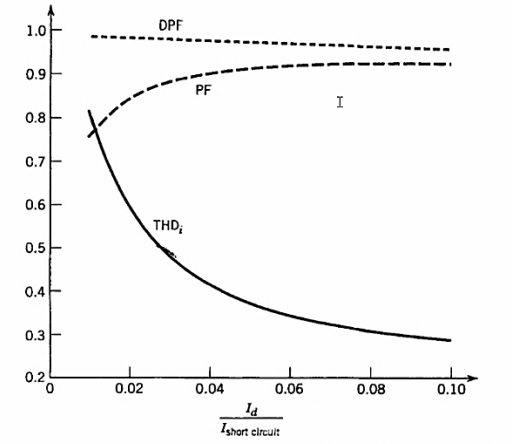

Figure 26: THD as a relation of load current and short circuit current. Reprinted with permission from [52]

In Figure 26, $I_{short-circuit}$ is defined by (36).

$$I_{short-circuit} = \frac{V_{in,LL,rms}}{\sqrt{3}.\omega L_s}, \text{ where } L_s = \frac{L_{choke}}{2} \tag{36}$$

Given I_d = 330 A. $\frac{I_d}{I_{short-circuit}}$ can be expressed in terms of L_s as $94L_s$. Hence it is can be seen from Figure 26 that a lower THD can be acquired using a higher value of DC link inductor. For 250 uH inductance the ratio $\frac{I_d}{I_{short-circuit}}$ is found to be 0.012. Hence the THD would be close to 70%. Hence, for a lower THD, the inductance value should be 5-10 times higher or 0.05-0.1 p.u. With a 0.1 p.u. inductance, the THD will be around 30% and value of L_{choke} is calculated to be 2.5 mH. Such an inductor can be too bulky for certain special applications. The proposed Active Inductor replaces this bulky inductor with a lighter system and has a much lower input current THD. The design specifications of the Active Inductor are shown in Table 5.

Table 5: Active Inductor specifications for the proposed design

Active Inductor Specifications	Rating
Commanded inductance (L_{ref})	2.5 mH
DC bus voltage (V_{dcBus}) in normal condition	500 V
DC bus voltage (V_{dcBus}) in undervoltage condition conon	1000 V
DC bus current (I_{dcBus})	330 A
Branch inductor (L_{act})	150 uH
DC bus capacitor (C_{dc})	1.5 mF
Switching speed (f_{switch})	40 kHz

Moreover, as the value of $L_{dc-link}$ is increased the DC link capacitor, $C_{dc-link}$ can be reduced to 0.15 mF. The proposed topology was simulated in PSIM for a 2.3 kV grid using the ASD specifications in Table 4.

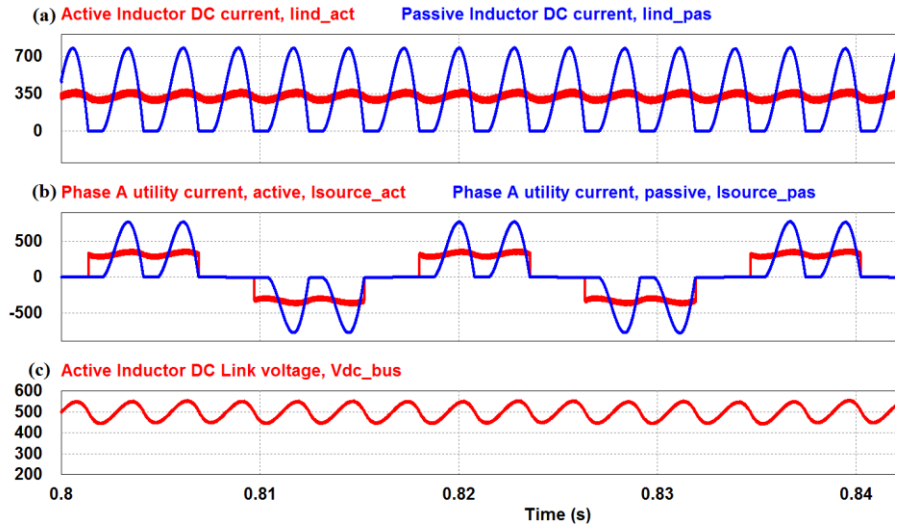

Figure 27: (a) Active Inductor current compared to passive inductor current, (b) Utility currents in phase A for active and passive systems, (c) Active Inductor DC bus voltage

Figure 27(a) shows the continuous current in Active Inductor ASD system (0.1 p.u. inductance) and discontinuous current in passive system (0.01 p.u. inductance). Because of the continuous current, the THD in utility current for the active system as shown in Figure 27(b) is found to be 32% compared to 70% THD in utility current in passive system.

4.2.3.1 DC bus capacitor design

The Active Inductor DC bus voltage required is less than 500 V during normal operation because the inductor terminal voltage, $V_{ind} < 500\,V$ as seen in Figure 28. Hence, the DC bus voltage, V_{dcBus} is regulated at 500V during normal operation.

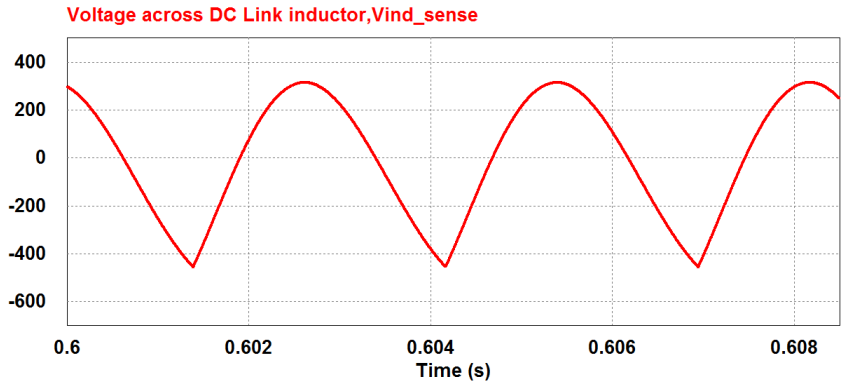

Figure 28: Voltage across DC link inductor in normal operation

However during fault conditions, the voltage across the inductor can be high. Figure 29 shows the DC link inductor voltage during a sag condition when a phase in the

utility grid shorts to zero. In such a case the Active Inductor DC bus Voltage V_{dcBus} needs to be higher in order to emulate this voltage across the Active Inductor terminals.

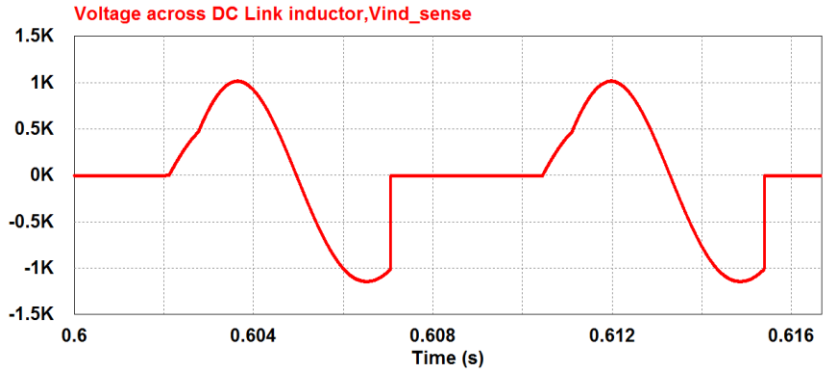

Figure 29: Voltage across DC link inductor in fault condition

V_{dcBus} can be regulated at a higher value during normal operation but it increases the current ripple in output. So, proper design should be done to meet the current ripple specifications. During a line fault condition, a higher value of voltage can be selected and the controller can increase the voltage accordingly. The DC bus capacitor should store enough energy to emulate the inductor. In ideal case with no losses in the Active Inductor, it should follow (37).

$$L_{ref} I_{load}^{\ 2} = C_{dc} V_{dcBus}^{\ 2} \tag{37}$$

Given that the Active Inductor will be slightly lossy compared to an actual inductor; the capacitor value has to be derated accordingly. According to (37) the C_{dc} value is found to be 1.1 mF. So, the capacitor can be selected as 1.5 mF after derating. (37) can also be used predict the boundaries of inductor value, L_{ref} that can be achieved

by the system. For example, if C_{dc} is chosen as 2 mF and V_{dcBus} can be regulated as high as 1000V depending on the derating of the capacitor, then $L_{ref,\max}$ is 18 mH or 0.72 p.u. Hence, the specifications of the system will determine the capacitance and voltage rating of the capacitor. Using (37) we can either choose to increase C_{dc} or V_{dcBus} voltage level or both. If we choose to increase V_{dcBus} while keeping C_{dc} constant we can regulate the V_{dcBus} voltage level at 600 V. Figure 30 shows this emulation of 5 mH inductance with V_{dcBus} being maintained at 600 V. Similarly, if the capacitance value is increased keeping V_{dcBus} as constant, C_{dc} can be increased to 2.2 mF. Figure 31 shows this emulation with V_{dcBus} being maintained at 500 V.

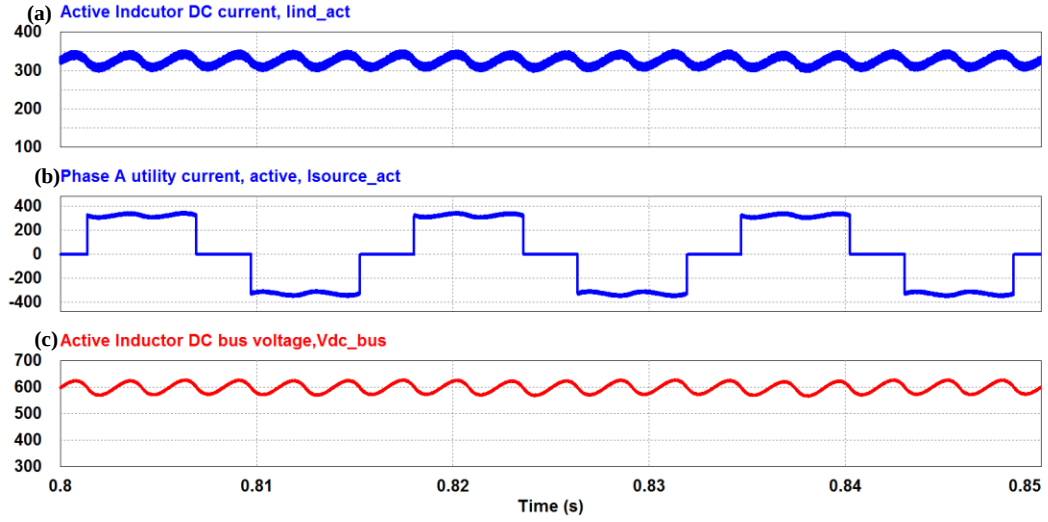

Figure 30: Emulation of 5 mH inductor with DC bus voltage at 600 V, (a) Active Inductor current, (b) Utility current in phase A, (c) Active Inductor DC bus voltage

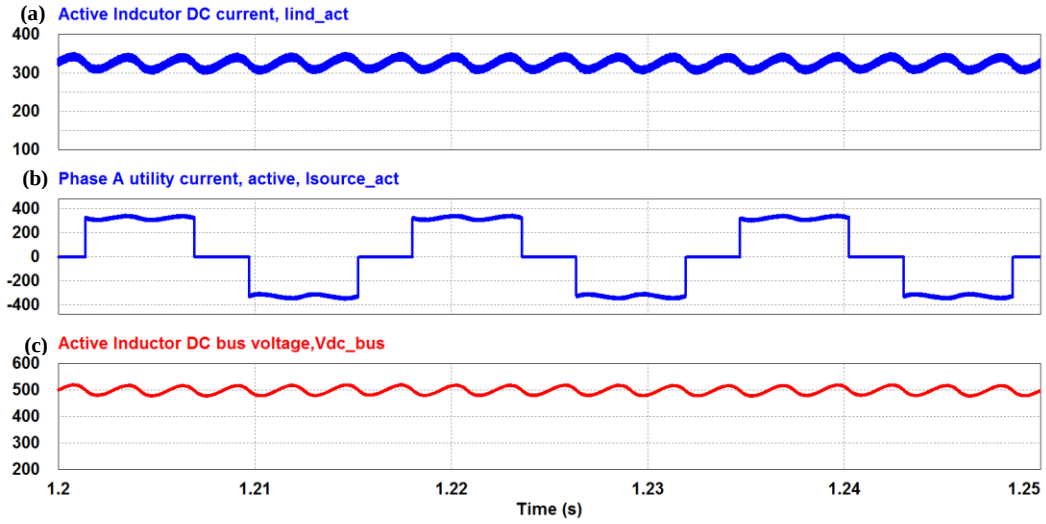

Figure 31: Emulation of 5 mH inductor with DC bus voltage at 500 V, (a) Active Inductor current, (b) Utility current in phase A, (c) Active Inductor DC bus voltage

4.2.3.2 Filter inductor design

Because of the switching at 40 kHz, there will be a high frequency ripple which can be absorbed by a small filter at the input. The load current will have a high frequency ripple envelope which is determined by (38).

$$V_{dcBus} = L_{filter} \frac{\Delta I_{ripple}}{DT_{switch}} \tag{38}$$

Since, the frequency of the current is 360 Hz and the high frequency switching occurs at 40 kHz, during the period, T_{switch}, the current can be assumed to be constant or DC in nature. In such a case, the duty ratio will be D = 0.5 which is used in (38). Assuming worst case 15% peak-peak ripple in the current, $\Delta I_{ripple} = 50A$. Then using (38) L_{filter} is calculated to be 150 uH. This high frequency ripple can be easily absorbed by high frequency filter on the utility side and motor inductance on the load side. In

case, a lower high frequency ripple is desired, (38) can be used to design the new filter inductor. For a 5% peak-peak ripple, the filter inductor is found to be $L_{filter} = 0.45mH$. Figure 32(b) shows lower ripple in utility current increasing the THD even further. Although the input current THD is lower, the filter inductor is bigger is size and the Active Inductor becomes bulky. Hence proper optimization should be done on this while choosing the filter inductor.

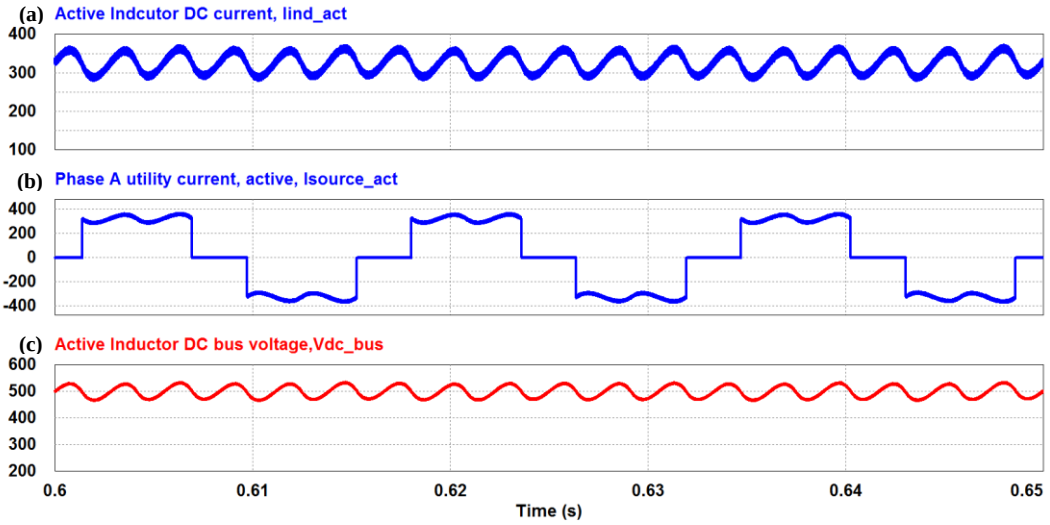

Figure 32: (a) Active Inductor current with lower high frequency ripple, (b) Utility current in phase A, (c) Active Inductor DC bus voltage regulated at 500 V

4.2.4 Simulation results

Simulation results for the ASD with step changes in load, input voltage and reference inductance value are presented.

4.2.4.1 Load step change

The system response of the system during a load step can be seen in Figure 33. Load is changed from 1 MW to 500 kW. The inner current control instantly adjusts the utility current as it reduces. Outer voltage control loop regulates V_{dcBus} to 500 V after initial dip in voltage.

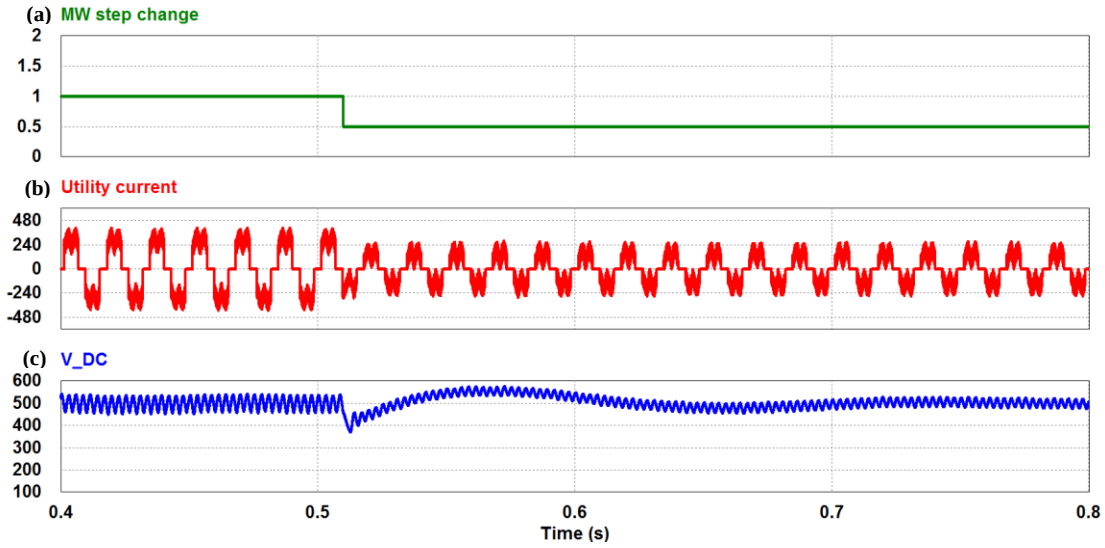

Figure 33: (a) Load step change, (b) Utility current in phase A, (c) Active Inductor DC bus voltage regulated at 500 V

4.2.4.2 Commanded inductance value step change

Figure 34 shows response of the system after step change in commanded inductance value, L_{ref} from 0.1 to 0.2 p.u. The line current THD reduces slightly to 31% from 32%. V_{dcBus} is quickly regulated to 600V to attain the energy required for increase in inductance value.

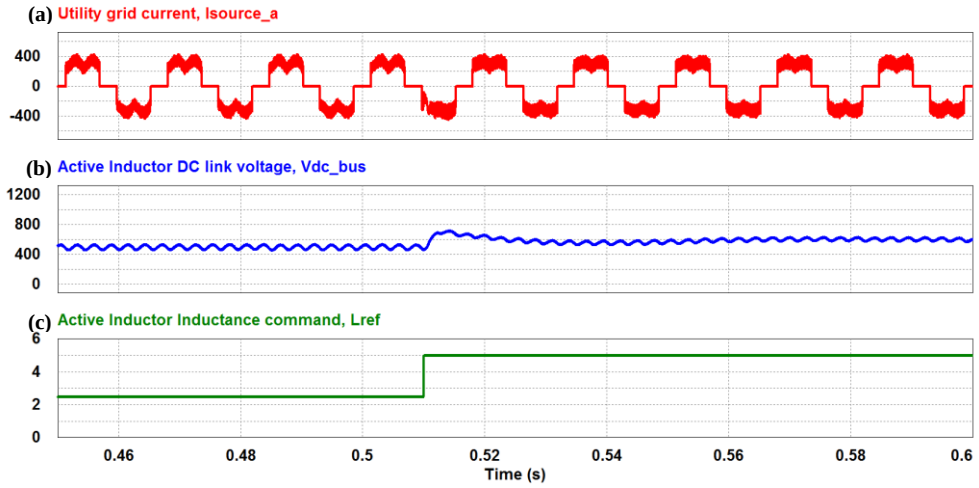

Figure 34: (a) Utility current in phase A, (b) Active Inductor DC bus voltage regulated at 500 V before step change and 600 V afterwards, (c) Step change in reference inductance value from 0.1p.u. to 0.2 p.u.

4.2.4.3 Input voltage step change

In Figure 35, Active Inductor emulates 0.1 p.u. inductance even after the grid fault at 0.5 s. The DC link current distortion increases and the line current THD increases from 31% to 39% after fault.

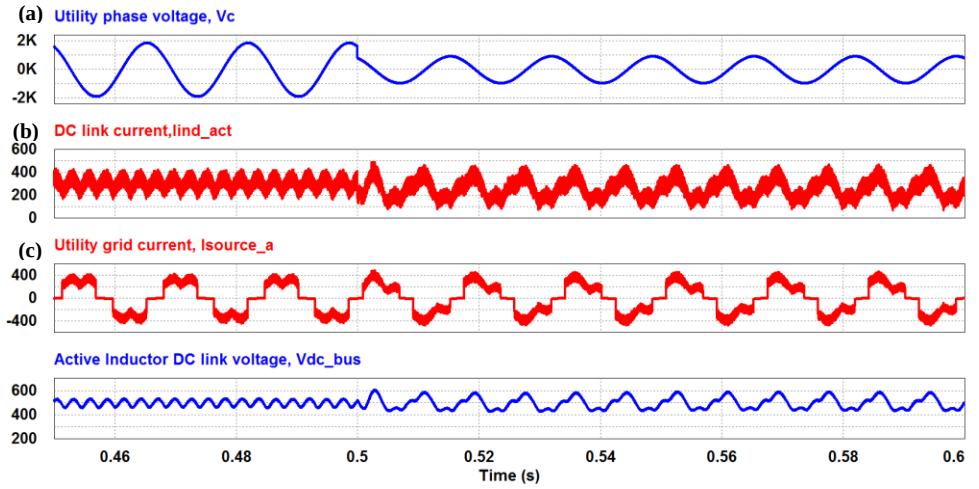

Figure 35: (a) Grid fault in phase C at 0.5 s, (b) Active Inductor DC link current, (c) Utility current in phase A (d) Active Inductor DC bus voltage regulated at 500 V

4.2.4.4 Improved fault response by dynamic inductance

In Figure 36, a similar grid fault is simulated at 0.5 s. However, after grid fault an inductance of 0.2 p.u. is emulated after the fault. V_{dcBus} is increased to 600 V in order to provide the energy required. The utility current THD increases from 32% to 34%. Hence, the system performance is better compared to the inductance value remaining same. Hence, the dynamic nature of the Active Inductor can be used to improve system performance during line faults.

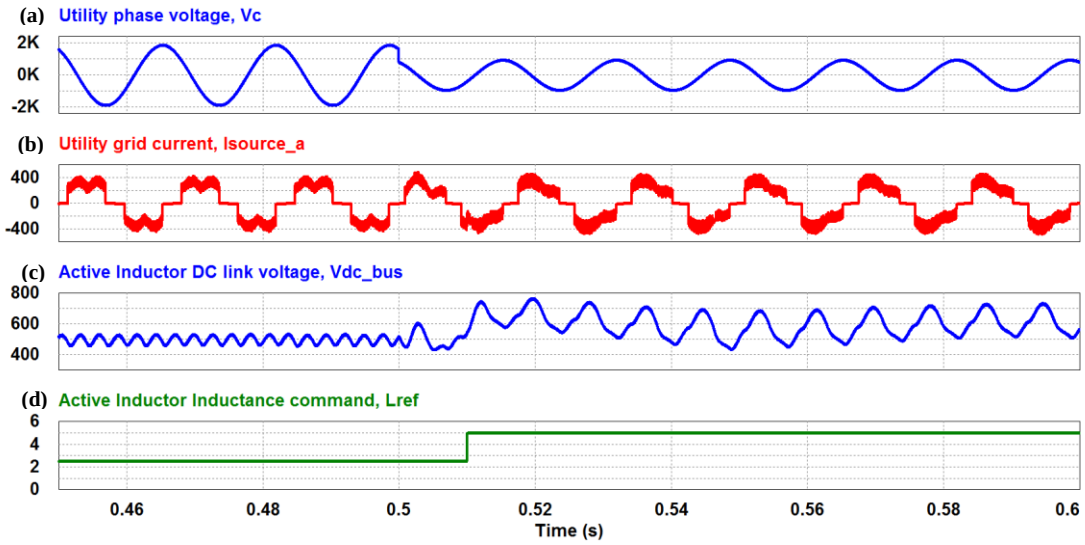

Figure 36: (a) Grid fault in phase C at 0.5 s, (b) Utility current in phase A, (c) Active Inductor DC bus voltage regulated at 500 V before fault and 600 V after fault, (d) Commanded inductance value changed from 2.5 mH to 5 mH

4.2.4.5 Improved performance in utility capacitor switching transients

A capacitor bank switching transient in utility causes overvoltage in DC link voltage of an ASD, which results in overvoltage trip [53]. The utility line inductance forms a LC resonance circuit with the switched capacitors and the resonating current has

to be absorbed by the DC link capacitor. The proposed Active Inductor can prevent this tripping by absorbing the high frequency current and reducing the overvoltage. As the transient is detected, the desired inductance value, L_{ref} is increased which dumps energy into the Active Inductor DC bus capacitor, thus reducing the amount of current that the DC link capacitor has to sink. To limit the overvoltage in Active Inductor DC bus capacitor, a bleeder resistor can be employed. As an example, the same ASD was simulated with capacitor switching transient at 0.5 s as shown in Figure 37. The DC link voltage in the active system does is limited to 3300 V while in the passive system, it reaches 3900 V.

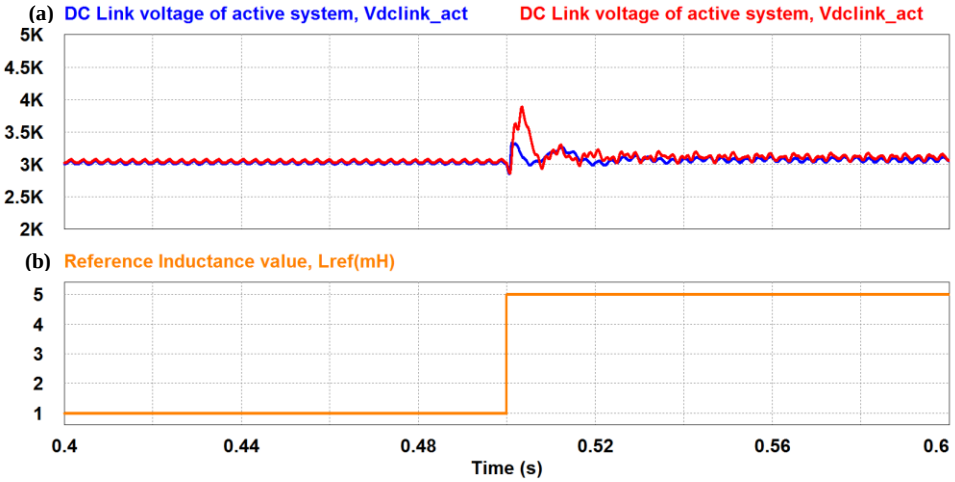

Figure 37: a) DC Link Voltage of active and passive systems with overshoot at capacitor switching transient, (b) Reference inductance value increased at time of event.

The Active Inductor DC bus voltage, V_{dcBus} is shown to be clamped by a bleeder resistor at 800 V in Figure 38.

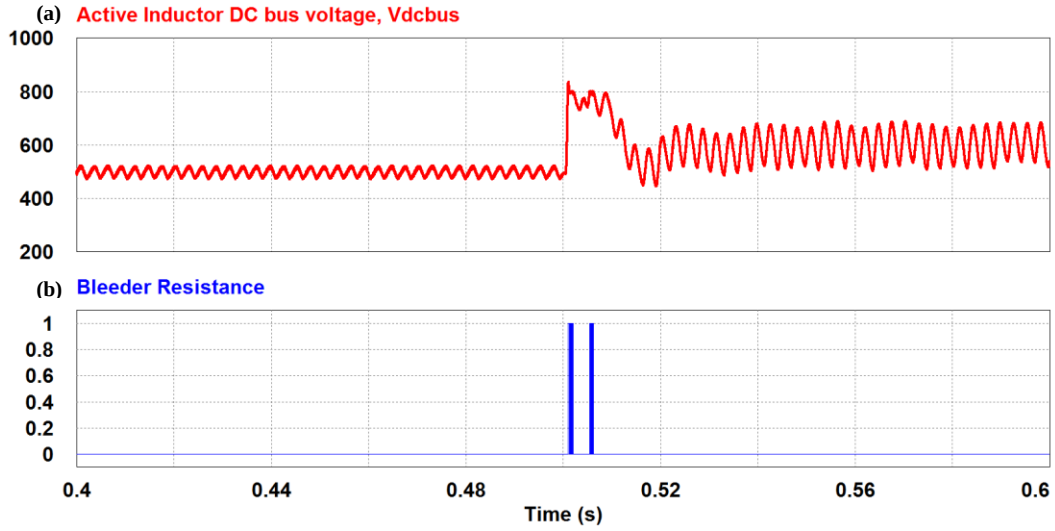

Figure 38: Active Inductor DC bus voltage capped at 800 V by bleeder resistor

4.2.5 Experimental results

A three phase diode rectifier with Active Inductor as DC Link reactor was built with a resistive load and tested with filter inductor, $L_f = 500\mu H$. A 200 W, three phase diode rectifier as shown in Figure 39 was also built with specifications shown in Table 6. The experimental setup is shown in Figure 40.

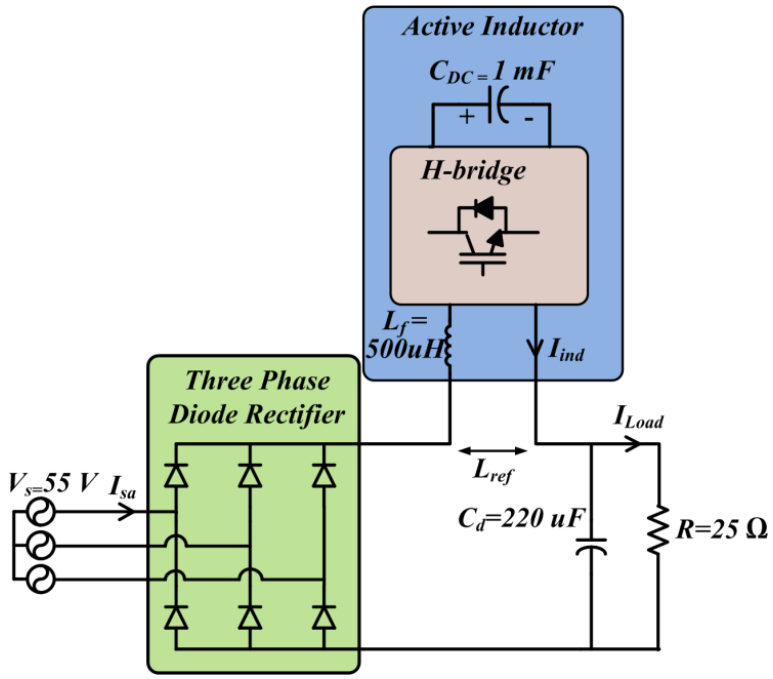

Figure 39: Circuit diagram for experimental setup

Table 6: Designed experiment specifications

Experiment Specifications	Rating
Input voltage, $V_{in,LL,rms}$	55 V
Output power, P_{out}	200 W
DC load current, I_{load}	2.8 A
Active Inductor, L_{ref}	500 uH, 2.5 mH
Filter inductor, L_f	500 µH
Active Inductor DC bus capacitor, C_{dc}	1 mF
Active Inductor DC bus voltage reference, $V_{dc,ref}$	15 V
ASD DC link capacitor, C_{dcLink}	220 uF

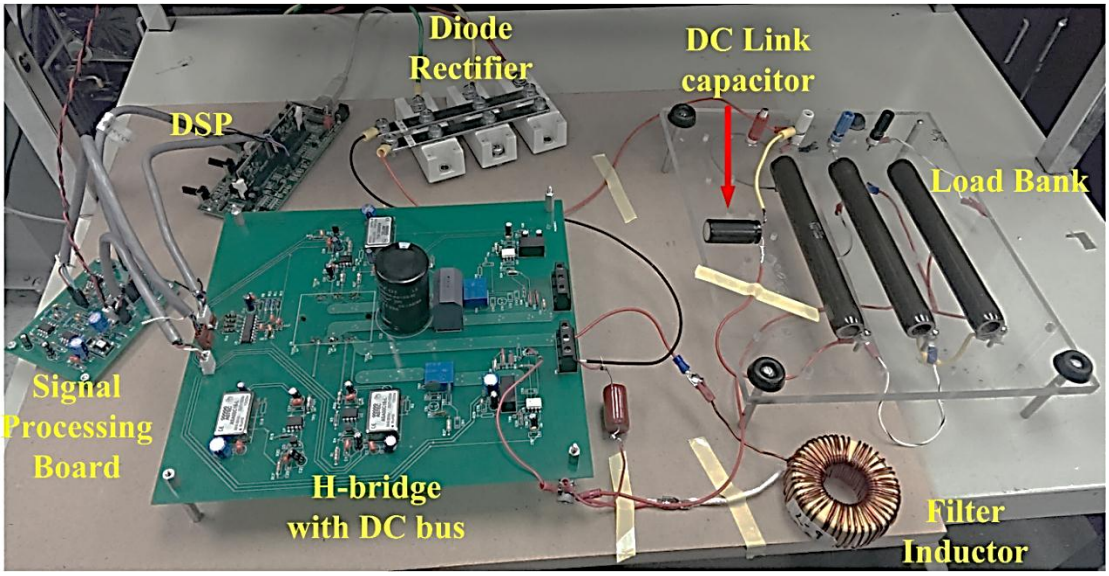

Figure 40: Experimental setup for 200 W, three phase diode rectifier with Active Inductor

Figure 41 shows the important waveforms for $L_{ref} = 500$ uH and Figure 42 for $L_{ref} = 2.5$ mH. It can be seen that the 6th harmonic in inductor current, I_{ind} and ripple on DC link voltage, V_{DClink} are significantly lower for the 8mH inductor. The pk-pk ripple in I_{ind} with $L_{ref} = 500$ uH is 5A whereas for $L_{ref} = 2.5$ mH, it is 3.6A. Similarly, the pk-pk ripple on V_{DClink} is 14.5V with $L_{ref} = 500$ uH and 4V with $L_{ref} = 2.5$ mH. The line power factor with $L_{ref} = 2.5$ mH is much better than $L_{ref} = 500$ uH as seen in Figure 42(b). The Active Inductor DC bus voltage, V_{dc} is seen to be regulated at 15 V.

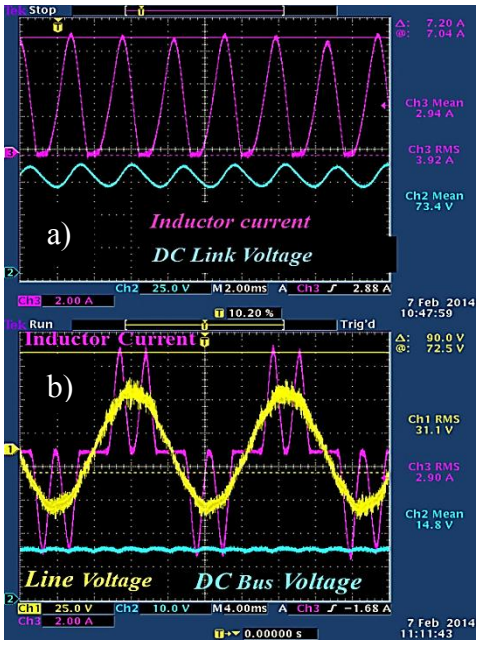

Figure 41: Experimental results showing Active Inductor waveforms for L_{ref} =500 uH. (a) Inductor current & DC link voltage, (b) Line current is distorted.

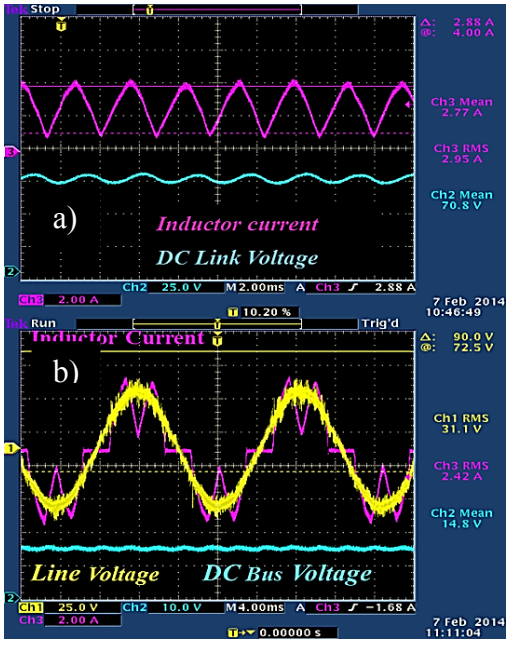

Figure 42: Experimental results showing Active Inductor waveforms for L_{ref} =2.5 mH. (a) Inductor current & DC link voltage, (b) Input power factor is higher.

Figure 43 shows a step change of L_{ref} from 2.5 mH to 500 uH. The Active Inductor DC bus voltage, V_{dc} is shown to be stabilized after a small reduction. The line current ripple also increases almost instantly. This shows that the current control has a quick reaction to change in reference inductance as shown in small signal modeling.

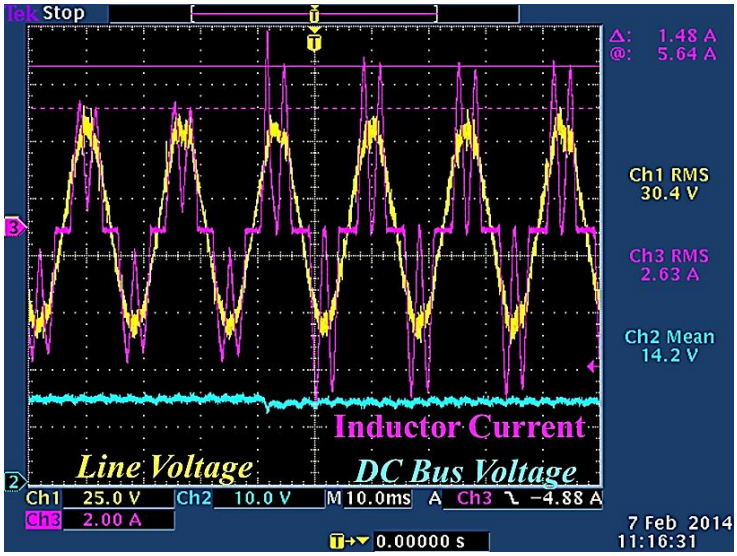

Figure 43: Step change of reference inductance value

4.2.6 System level design

The utility grid is not directly connected to the ASD for a cold startup. In order to prevent huge inrush current into the ASD DC link capacitor, usually a soft-charge resistor, as shown in Figure 44 is used. This limits the current while the capacitor gets charged up. Once, the capacitor is charged to required value, the soft-charge resistor is shorted out.

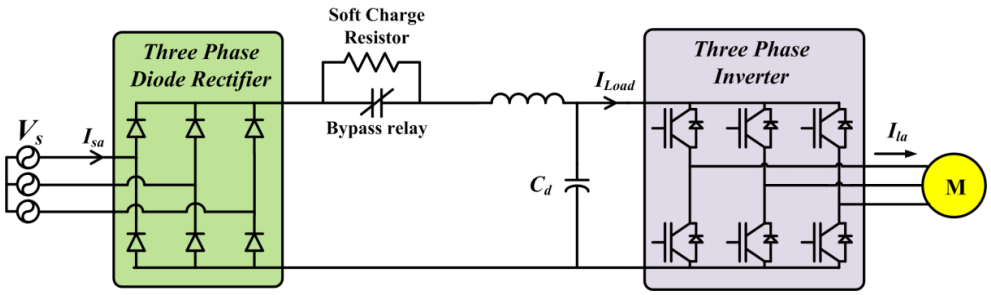

Figure 44: ASD with a soft-charge resistor and bypass relay

When the Active Inductor replaces the passive DC link reactor, the switches in the H-bridge during the time of startup will be subject to a high voltage stress which might lead to failure. To prevent this, a startup sequence needs to be incorporated for ASDs which use Active Inductor. The H-bridge of the Active Inductor needs to be shorted out using a triac as shown in Figure 45. The voltage stress across the switches will become zero at the time of startup. Once the DC link capacitor, C_d is soft charged, the triac can be turned off and the gating signals to the H-bridge can be started to charge the Active Inductor dc bus capacitor, C_{DC}. Hence, this startup sequence is required to prevent failures in the Active Inductor setup.

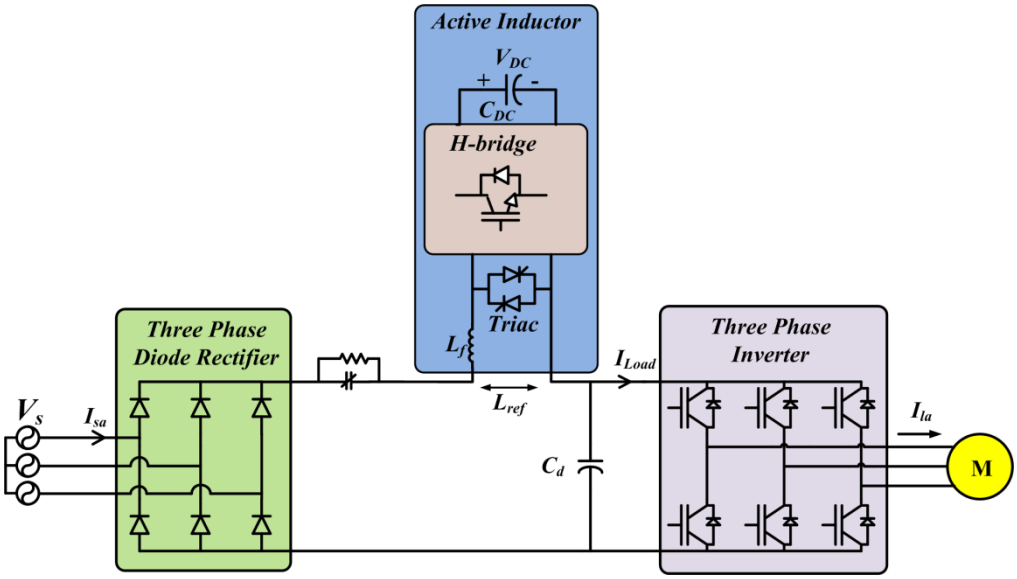

Figure 45: Active Inductor as DC link reactor in ASD with triac

Another event when the triac can become useful is during an inverter short. When there is a short in the inverter terminals, there is a huge overcurrent and the H-bridge switches will be destroyed with this huge current stress. As soon as the overcurrent is detected, the triac can be turned on and the switches can be protected. Hence the triac serves a dual purpose.

4.2.7 Zero Voltage Switching (ZVS) switching technique

High frequency operation of hard-switched power converters entails a huge amount of switching losses. In DC-DC power supplies with high switching frequency resonant converter topologies are preferred [46]. Resonant topologies employ the energy stored by leakage inductance of the transformer. Usually, for implementing these topologies, extra active and passive components are required. However, the gains made

in efficiency and size reduction of heat sink compensate for the increased component count. Hence, ZVS and Zero Current Switching (ZCS) techniques are preferred.

Circuit parasitics are usually considered lossy elements in a converter. Switching losses are enhanced due to the parasitics in high frequency high power operation. Generally, snubbers are required to decrease the current and voltage spikes adding further to the losses. In [46] a full bridge PWM converter is proposed in which ZVS for all switches is achieved by using the circuit parasitics for resonant switching. This reduces the need for extra passive components. To achieve ZVS, the two legs of the full bridge are operated with a phase shift. The energy stored in leakage inductance is used to discharge the output capacitances of MOSFETs and the antiparallel diode of the MOSFET is forced to conduct before the MOSFET turn on. Hence, ZVS turn on is achieved.

For the Active Inductor topology, a DC current is always flowing through the topology. This energy can be used to charge and discharge the parasitic capacitances and similar behavior as shown in [46] can be achieved. A model of the H-bridge with the parasitic capacitances is shown in Figure 46.

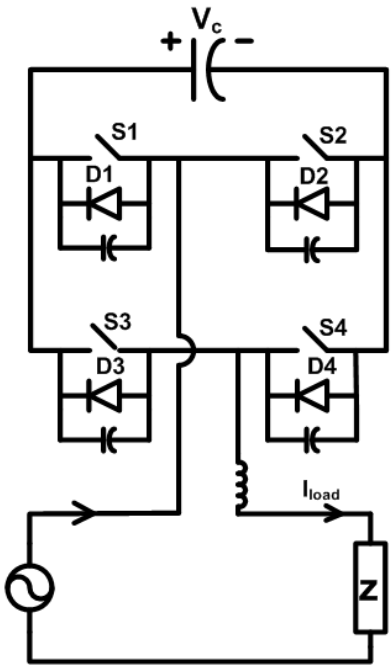

Figure 46: Parasitic model employed for ZVS scheme

The modes of operation of this technique are as follows:

1) Mode I: In this mode switch S2 and S3 are turned on and the DC Link Capacitor is being discharged as shown in Figure 47. The current flow is shown with blue arrows. The parasitic capacitance across switches S1 and S4 are charged to value V_c. In order to achieve ZVS turn on for the second leg, both the parasitic capacitors have to be discharged.
2) Mode II: In the beginning of Mode II (end of Mode I), S2 is turned off and S3 is kept turned on as shown in Figure 48. Now the current which was earlier passing through switch S2 is forced to take either of the 2 paths maintaining (39)
    i) Charge the parasitic capacitance of switch S2
    ii) Discharge the parasitic capacitor of switch S1

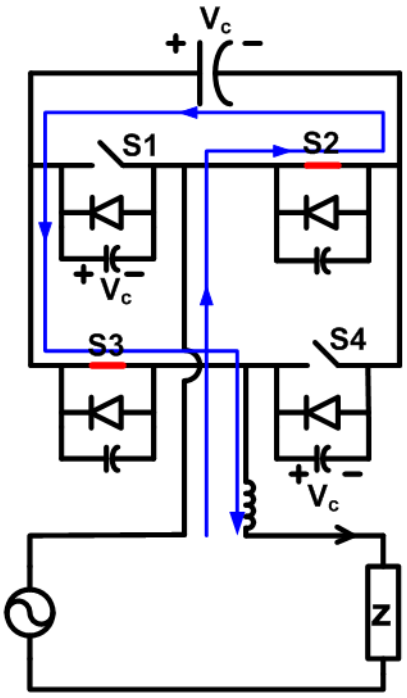

Figure 47: Mode I of ZVS operation

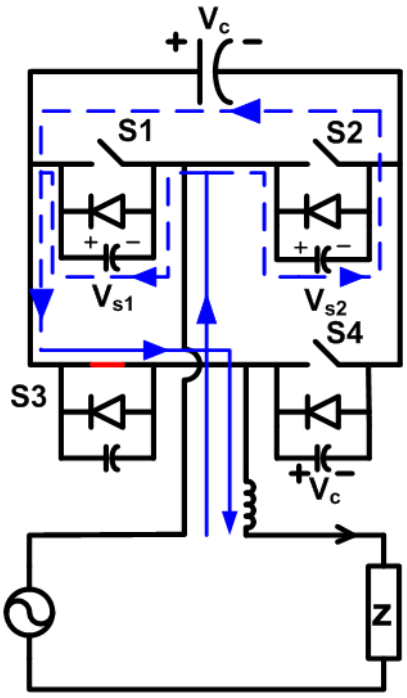

Figure 48: Mode II of ZVS operation

As the Capacitor across S1 is discharged or V_{S1} becomes 0 the voltage across the antiparallel diode, D1 becomes zero. Now the conditions required for the D1 to conduct are being met and current starts flowing across D1. With this the voltage across S1 is zero and it can be turned on in ZVS.

$$V_{S1} + V_{S2} = V_c \tag{39}$$

3) Mode III: Now, the switch S1 is turned on with ZVS as shown in Figure 49. The current which was flowing through the Diode D1 is now shared by both D1 and S1. The current starts to flow bypassing the DC link capacitor. This mode of operation should remain transitory in nature as now there is no control of the

Active Inductor. In other words, the inductance value becomes the filter inductor value and this could lead to current surges.

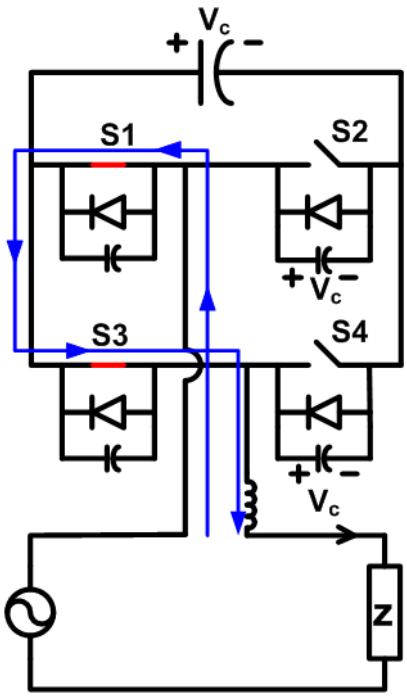

Figure 49: Mode III of ZVS operation

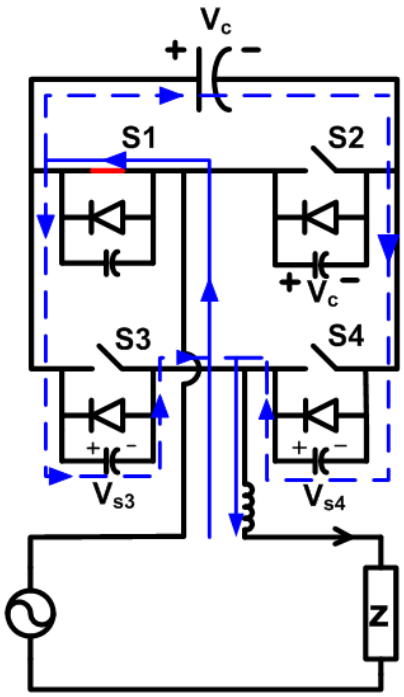

Figure 50: Mode IV of ZVS operation

4) Mode IV: In the beginning of Mode IV, switch S3 is turned off. Now the current passing through S1 has two paths it can take as shown in Figure 50.

   i) Charge the parasitic capacitance of switch S3

   ii) Discharge the parasitic capacitance of switch S4

Once the parasitic capacitance of S4 is discharged, all the current can now pass through Diode D4, the antiparallel diode of switch S4.

5) Mode V: Once diode D4 is conducting, switch S4 can be turned on in ZVS and then current will flow as shown in Figure 51 charging the DC link capacitor.

As described in the five modes, the current was transferred from one leg to the other of the full bridge. ZVS turn on was achieved for switches S1 and S4 while S2 and S3 were hard switched when being turned off. The similar process can be used to turn on switch S2 and S3 by repeating the modes explained for these switches.

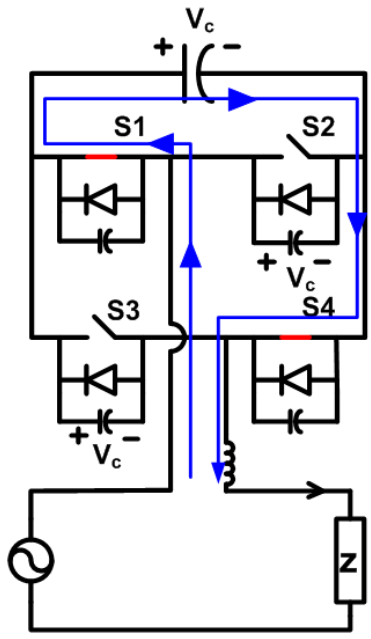

Figure 51: Mode V of ZVS operation

4.3 Active Inductor to replace utility side inductor in LCL filter in PV farm

LCL filters are extensively used in utility interface of energy sources. It can provide a better decoupling between the filter and the grid with small L and C values

compared to a LC filter. It produces lower ripple current distortion across the grid-side inductor since the current ripple is reduced by the capacitor. A control strategy for obtaining a low harmonic distortion in a distribution network fed by an LCL filter based three-phase VSI system has been explored in [54] . Figure 52 shows the typical circuit diagram for such a system.

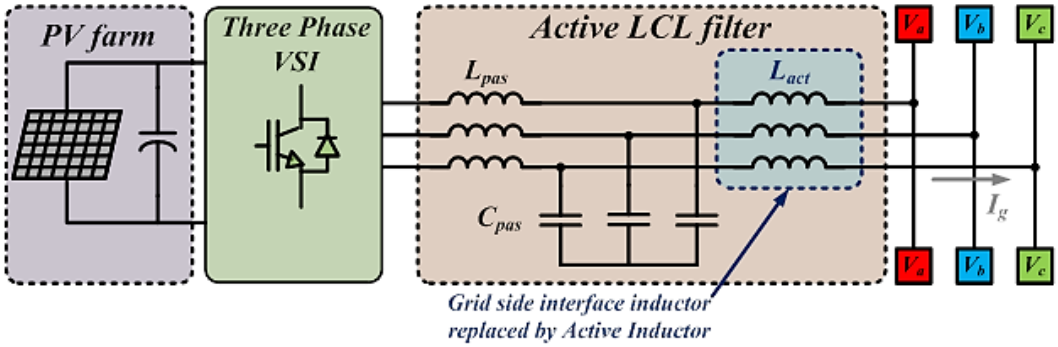

Figure 52: PV farm connected to the grid through an active LCL filter

Though proper design of the LCL filter, the quality of the current injected in the grid, I_g, can be significantly improved to have a low THD (≈2%). The proposed Active Inductor, L_{act}, can replace this large inductor leaving the remaining components to be in passive, C_{pas} and L_{pas}, as shown in Figure 52. With the added flexibility to tune the LCL filter due to the presence of the Active Inductor, the solar PV inverter switching frequency can be altered to achieve high conversion efficiency under wide variation of solar insolation.

4.3.1 Low Voltage Ride Through (LVRT)

A PV farm would be required to remain operational during a grid fault as shown in Figure 53. During unbalanced voltage sags, the grid codes require PV farm utilities to reduce the active power and supply reactive power to support the grid till the grid comes back to normal.

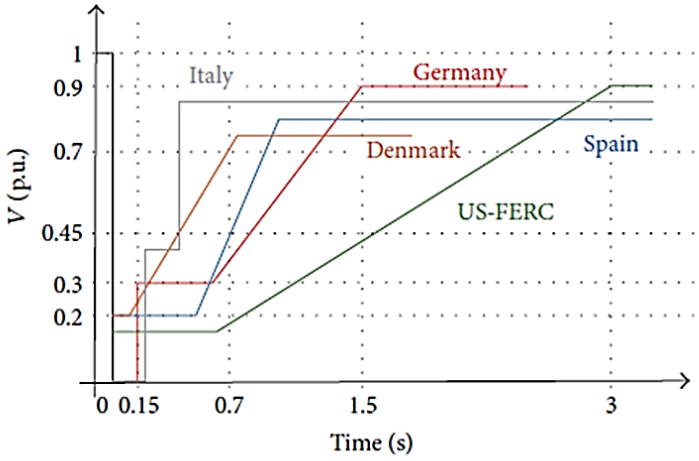

Figure 53: LVRT specifications in different countries. Reprinted with permission from [55]

In a conventional PV farm, when there is a fault at the utility side, the voltage at the output of the inverter drops. The output power of the inverter can be reduced by varying the modulation index, once the fault has been detected by the central controller. The duration taken by the controller to react can cause the utility current to rise and shutdown the system under overcurrent protection. This issue needs to be overcome while incorporating LVRT capability. One way to reduce the current surge is by

dumping the excess energy into a DC-link chopper. If the energy mismatch is large, then the chopper rating has to be sufficiently high.

In the proposed design, the passive components in an LCL filter can be selected such that the utility side inductor is large. When a fault occurs in the system, the central controller increases the inductance value of the Active Inductor momentarily to a large value. This increases the impedance of the line and limits the current to a safe value. This happens simultaneously with the inverter reducing the modulation index to decrease the amount of power supplied. Hence, the overall response of the system becomes faster than the conventional system with a passive utility side inductor. Once the power generated by the farm is sufficiently reduced, reactive power has to be fed to the grid so that once the fault is cleared, the PV farm can start supplying to the grid at rated power. The DC link capacitor of the Active Inductor has to be derated for LVRT. The basic rule followed by the DC Link capacitor of the Active Inductor is shown in (40).

$$L_{ref} I_{load}^{\ 2} = C_{dc} V_{dc}^{\ 2} \tag{40}$$

As the L_{ref} inductance value is being increased and the reactive current is kept similar in magnitude to active current in normal conditions, either the capacitance value or the voltage rating of the capacitor has to be high enough to accommodate the extra energy.

4.3.2 Design example: PV farm inverter

The specifications required for the PV farm inverter are shown in Table 7.

Table 7: PV farm specifications

Specification	Rating
Power	100 kW
Input voltage	800 V_{dc}
Grid voltage	480 V_{rms}
Switching frequency	3.6 kHz
Resonant frequency	<1.5 kHz
L_2 voltage to inverter output(nth harmonic)	<5%
Grid current to Inverter output voltage (nth harmonic)	<2%

The resonant frequency was selected to be less than 1.5 kHz to attenuate the harmonics at 3.6 kHz. To improve the harmonic rejection of the filter, the following specifications were chosen.

$$\frac{V_{L_1,n}}{V_{inv,n}} < 1.05 \tag{41}$$

$$\frac{V_{L_2,n}}{V_{inv,n}} < 5\% \tag{42}$$

$$\frac{I_{grid_1,n}}{V_{inv,n}} < 2\% \tag{43}$$

where n = 60 ($\frac{f_{switch}}{f_1}$)

Rejection of harmonics at switching frequency at PV farm side inductor L_1 is necessary to reduce the voltage harmonics subjected to the grid side inductor L_2. The Active Inductor which aims to emulate this inductor requires emulated voltage to have

lesser high frequency terms in order to keep the Active Inductor switching frequency reasonable. The grid current should have low harmonics as shown by (43).

In order to design the LCL filter, the circuit shown in Figure 54 is used.

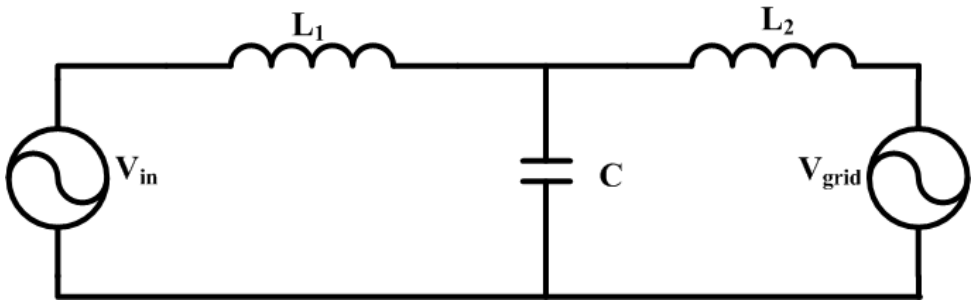

Figure 54: Circuit diagram for LCL design

The following are used to select the individual passive components of the LCL filter.

$$\frac{I_{grid,n}}{V_{inv,n}} = \frac{1/nsL_2}{1+L_1\left(\frac{1}{L2}+n^2\omega^2C\right)} \tag{44}$$

$$\frac{V_{L_1,n}}{V_{inv,n}} = \frac{1}{1+\frac{1}{L_1\left(\frac{1}{L2}+n^2\omega^2C\right)}} \tag{45}$$

$$\frac{V_{L_2,n}}{V_{inv,n}} = \frac{1}{1+L_1\left(\frac{1}{L2}+n^2\omega^2C\right)} \tag{46}$$

Resonant Frequency, $f_r = \frac{1}{2\pi}\sqrt{\frac{L_1+L_2}{L_1L_2C}}$ (47)

Table 8: Filter performance with varying values of inductance and capacitance

Case No.	L_1 (uH)	L_2 (uH)	C (uF)	$\frac{I_{grid_1,n}}{V_{inv,n}}$	$\frac{V_{L_2,n}}{V_{inv,n}}$	f_r (Hz)
1	170	170	300	1	4.15	1001
2	50	300	300	1.7	15.3	1403
3	100	200	300	1.4	7.2	1125
4	200	100	300	1.6	3.6	1125
5	250	50	300	2.5	3.1	1423
6	300	50	300	2.15	2.6	1402
7	200	200	200	1.1	5.4	1125
8	200	200	50	4.3	3.2	2250

Table 8 shows the value of performance criteria with varying values of passive components. It can be seen than 2 of the 7 selected variations meet the design criteria. If there too much difference between L_1 and L_2 value, the performance of the LCL filter is not optimum. A smaller PV side inductor, L_1 will increase the voltage harmonics on L_2, the grid side inductor. On the other hand, a smaller grid side inductor will increase the grid current harmonics. Moreover, if the individual passive components are large the size of LCL filter is similar to an LC filter. A better LCL design methodology is to have almost similar values of inductances on both sides.

Moreover, looking at (46), for a given value of capacitance, the smallest cutoff frequency can be obtained when $L_1 = L_2$. It can be seen that when this criteria is met, the cutoff frequency is lowest. This ensures a high quality of grid current as the attenuation at switching frequency is best possible. Hence, for the design purpose, LCL values in Case#1 is selected.

Table 9: Specifications of Active Inductor to emulate the grid side inductor

Active Inductor Specifications	Rating
DC bus voltage, V_{dcBus}	300 V
DC bus voltage during grid fault	1000 V
DC bus current, $I_{dcBus,rms}$	220 A
Branch inductor, L_f	75 uH
Active Inductor DC bus capacitor, C_{dc}	1 mF
Switching speed, f_{switch}	40 kHz

Table 9 shows the specifications of Active Inductor to replace the grid side inductor. To design the Active Inductor DC bus capacitor, C_{dc}, information about the inverter response during voltage fault conditions are used. Here the inverter takes τ =10 ms to respond. Hence, for 10ms, all the energy needs to be dumped in the capacitor.

$$\frac{1}{2} C_{dc} V_{dcBus}^{\ 2} = \frac{1}{2} \tau . P_o \tag{47}$$

V_{dcBus} is also expected to swell upto 1000 V during fault. Using (47) C_{dc} is calculated to be 1 mF. For branch inductor, L_{act} the high frequency ripple across the envelope can be set to a desired value, $\Delta I_{ripple} = 50A$.

$$V_{dcBus} = L_{filter} \frac{\Delta I_{ripple}}{DT_{switch}} \tag{48}$$

Using (48) L_{act} is calculated to be 75 uH. A single phase PV farm generating 100 kW at full insolation was simulated in PSIM. Figure 55 shows the steady state operation in comparison to a passive LCL filter system.

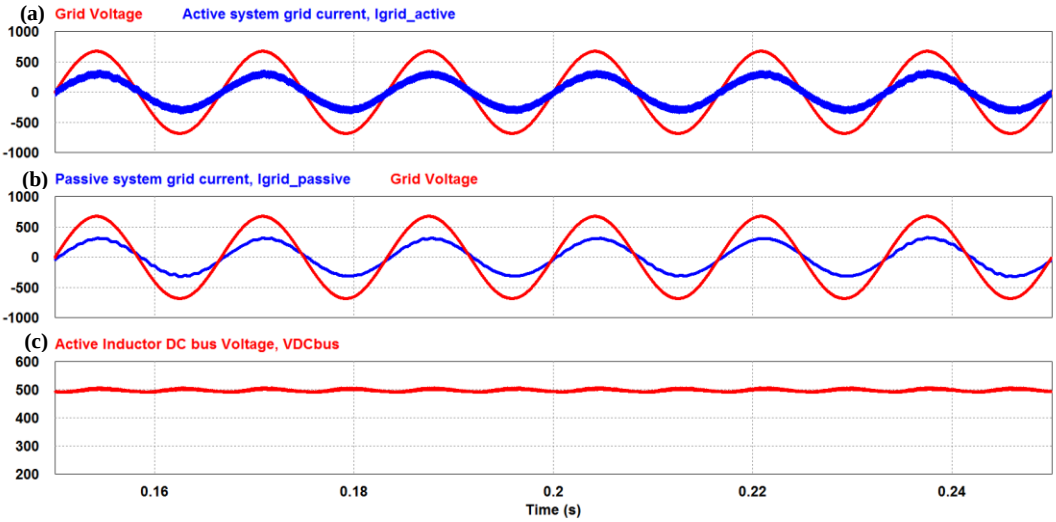

Figure 55: Active Inductor LCL performance in normal conditions (a) Grid voltage and grid current in active system, (b) Grid voltage and grid current in passive system, (c) Active Inductor DC bus voltage regulated at 500 V

The grid current THD in active system is slightly higher than the passive system but less than 5%. Moreover, the high frequency ripple can be absorbed by a small filter at the utility.

4.3.2.1 LVRT simulation

The grid side Active Inductor prevents the rise of grid current to overcurrent level and protects the components of the converter. Figure 56 shows the response of the system when the single phase grid is grounded at fault. The passive system shows a spike in grid current which is not seen in the active system because of the increased commanded inductance value, L_{ref} to 850 uH from 170 uH. The energy from the PV farm which is converted by the inverter before it reacts to the fault is absorbed by the Active Inductor DC Bus capacitor, C_{DCbus}.

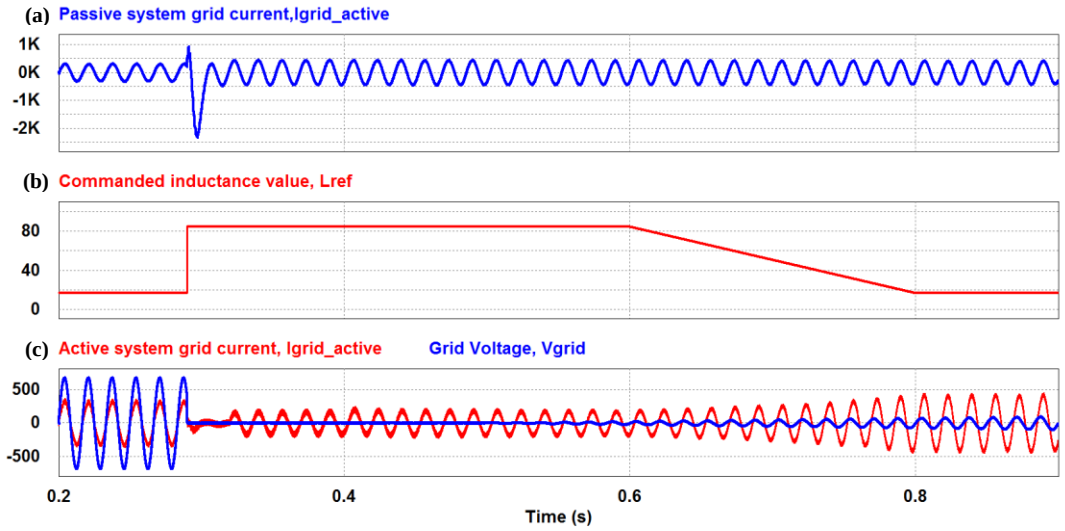

Figure 56: System response during grid fault (a) Passive system grid current, (b) Commanded inductance value during fault in uH, (c) Active system grid current and voltage

Once the grid voltage starts increasing, L_{ref} starts to decrease, which is eventually reduced to 170 uH. While the grid voltage is low, the system also supplies with reactive current and keeps the system online as per LVRT requirements.

4.4 Other applications

Thyristor based Current Source Rectifier (CSI) employs a large inductor to maintain a DC output current. However, with a varying firing angle of the thyristors, the distortion in the current also varies. The Active Inductor topology can replace this passive inductor as shown in Figure 57 and dynamically change its inductance value to maintain the quality of current.

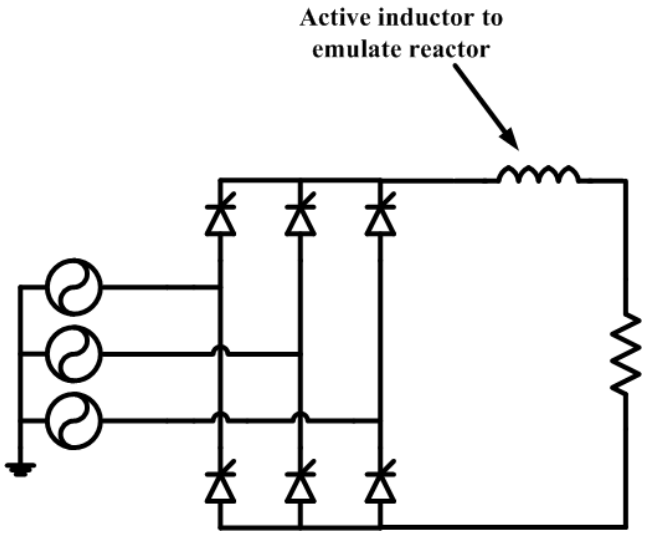

Figure 57: Thyristor based CSI with Active Inductor emulating the reactor

4.5 Conclusion

The possible applications of the Active Inductor have been explored. The Active Inductor can replace the DC Link reactor in an LC filter of an ASD, utility side inductor of an LCL filter for a PV farm inverter and Dc link reactor of thyristor based CSI. The overall system architecture of each application along with design methodology for system components has been described. The advantages of dynamic inductance in each application are discussed. A design example of ASD system has been presented. Simulation and experimental results have been shown to validate the concept and portray the robustness of the designed controller.

5. WEIGHT, SIZE AND LOSS ANALYSIS

5.1 Introduction

The Active Inductor emulated a 0.1 p.u. inductance (2.5 mH) in the ASD design example. It was also shown that usually a smaller inductor at 0.01 p.u. (250 uH) is used for discontinuous conduction. The proposed Active Inductor system has been analyzed in terms of weight, size and losses for the DC link reactor in the diode rectifier fed ASD system. Corresponding analysis has been done for passive systems. A comparison between all the options is done to portray the size and weight gains over passive systems.

5.2 Passive inductor design and analysis

In order to design an inductor, (49-50) are followed:

$$nI_{\max} = \frac{B_{\max} l_g}{\mu_o} \tag{49}$$

$$L = \frac{\mu_o A_c n^2}{l_g} \tag{50}$$

where, n – number of turns; $I_{\max}$ – maximum winding current (A); $B_{\max}$ – maximum flux density (T); l_g – air gap (mm);

L – inductance (H) ; A_c - core area; μ_o – permittivity

There are several choices for a low frequency high power inductor. However the most common choice is of silicon steel because of its low cost. The required properties of silicon steel are shown in Table 10.

Table 10: 0.1 p.u. passive inductor specifications

Parameters	Values
Inductance	2.5 mH
Peak current	400 A
RMS current	350 A
Density, $\rho_{Si-Steel}$	7 g/cm^3
Saturation flux density, B_{sat}	1.5 T
Design maximum flux density, $B_{\max}$	1 T
Selected Air gap, l_g	10 mm

Using the above parameter values in (49) and (50) other parameters can be determined. From (49), substituting the known parameters, number of turns, n can be found to be $n=20$. Cross sectional area, A_c can be found from (50) to be $A_c = 500$ cm^2. Assuming that the cross Sectional Area is kept as a square, side of cross section area is found to be, $l_{cs} = 22.5$ cm.

Generally, for high power applications, the wire includes wire insulation and core insulation; hence the winding wire can occupy only a certain percentage of the vacant area or the fill area. The parameter which determines the ratio of area available for wires is fill ratio(f) [56]. Rest of the area is occupied by wire and core insulation. For such

high power application fill ratio can be selected as $f = 0.1$. Wire thickness for 400 A current can be selected as 1 inch (23 mm) diameter. So wire area,

$$A_{wire} = \pi r^2 = 16.7 \text{ cm}^2 \quad (51)$$

Assuming $A_{wire} = 20$ cm^2, total fill area required can be found by (52). Again, assuming, the fill area to be a square, each side of the square is calculated to be $l_{side} = 63.2$ cm.

Total fill area required, $A_{fill} = \frac{A_{wire}.n}{f} = 4000 \text{ cm}^2 \quad (52)$

Mean length of the core, L_{mean}, can be calculated now to be, $L_{mean} = 344$ cm. Now, the weight of the core, W_{core} can be calculated from the parameters.

$$W_{core} = L_{mean}.A_c.\rho_{Si-Steel} = 1295 \text{ kg} \quad (53)$$

Also, weight of Copper winding can be found after knowing the circumference.

$$A_{wire}.n.Circumference_{core}.\rho_{Cu} = 288 \text{ kg} \quad (54)$$

Table 11: Calculated parameters for 0.1 p.u. passive inductor with silicon steel core

Parameter	Value
Selected air gap, l_g	10 mm
Number of turns, n	20
Cross-sectional Area, A_c	500 cm^2
Mean length, L_{mean}	344 cm
Fill area, A_{fill}	4000 cm^2
Weight of core, W_{core}	1295 kg
Total weight	1583 kg
Total volume	316100 cm^3

Following similar design methodology, the 0.01 p.u. passive inductor can be designed as shown in Table 11.

Table 12: 0.01 p.u. passive inductor specifications

Parameters	Values
Inductance	250 uH
Peak current	800 A
RMS current	350 A
Density, $\rho_{Si-Steel}$	7 g/cm^3
Saturation flux density, B_{sat}	1.5 T
Design maximum Flux Density, $B_{\max}$	1 T
Selected Air gap, l_g	10mm

Table 13: Calculated parameters for 0.01 p.u. passive inductor

Parameter	Value
Selected air gap, l_g	10 mm
Number of turns, n	10
Cross-sectional area, A_c	200 cm^2
Mean length, L_{mean}	235 cm
Fill area, A_{fill}	2000 cm^2
Weight of core, W_{core}	329 kg
Total weight	431 kg
Total volume	47000 cm^3

Table 12 and 13 show the specifications and calculated parameters for the 0.01 passive inductor. The volume and weight of 0.01 p.u. inductor is significantly lesser than

the 0.1 p.u. inductor. However, because of discontinuous current, the maximum current is higher at 800 A. This high peak current needs a larger volume of core compared to an inductance of similar value but low peak current.

5.3 Active Inductor design and analysis

The Active Inductor consists of SiC full bridge, filter inductor and DC Link Capacitor. In order to find the weight and size of the complete system, each component has to be designed for the desired specifications to find actual gains in size and weight.

5.3.1 Filter inductor

There is a huge demand for compact magnetic design which can meet efficiency targets of several industries. Usually in a hard-switched dc-dc converter, magnetics occupies maximum space and thus reduction of size of magnetics is important for overall reduction of size [57]. Important parameters which determine the choice of core are determined by operating dc current, current ripple, air-gap length, operating frequency, ambient and heat sink temperatures. Amorphous metal and powder core have been used for high frequency magnetics. Nanocrystalline material has excellent magnetic parameters and is superior to these materials. However, there are problems with manufacturability which have not been solved yet and prevent the industries from adopting this new technology [57]. However, it is expected that these problems will be solved and nanocrystalline materials are expected to become a preferred solution in future. Figure 58 shows that Vitoperm 500F (nanocrystalline) has significantly lower

losses at high saturation flux densities compared to amorphous metal and powder iron core.

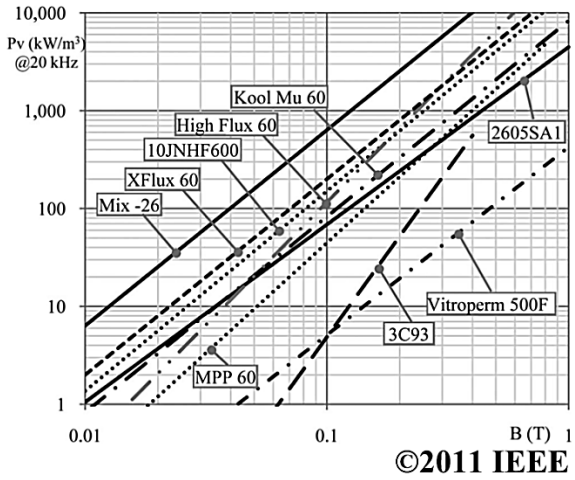

Figure 58: Relative core losses at 20 kHz. Reprinted with permission from [58]

Hence, for the high frequency filter inductor a nanocrystalline core – Vitoperm 500F is selected. Table 14 and 15 show the filter inductor specifications and calculated parameters respectively.

Table 14: Filter inductor specifications

Parameters	Values
Inductance	150 uH
Peak current	400 A
RMS current	350 A
Density, $\rho_{vitoperm}$	7.7 g/cm^3
Saturation Flux Density, B_{sat}	1.2 T
Design Max Flux Density, $B_{\max}$	1 T
Selected Air gap, l_g	3 mm

Table 15: Calculated parameters of filter inductor

Parameter	Value
Selected air gap, l_g	3 mm
Number of turns, n	6
Cross-sectional area, A_c	120 cm^2
Mean length, L_{mean}	178.5 cm
Fill area, A_{fill}	1200 cm^2
Weight of core, W_{core}	137.5 kg
Total weight	170 kg
Total volume	25000 cm^3

5.3.2 DC bus capacitor

The DC bus capacitor could be selected as a metalized polypropylene film capacitor to reduce capacitance drift for high temperatures and increased reliability [59] Polypropylene film capacitors can be used for high power applications. Commercial products are now available which are used for DC filtering for high frequency operation and high rms current [48]. The selected capacitor for this purpose is AVX – TRAFIM. Choosing from the product portfolio available, 2 capacitors of 1250 uF can be setup in parallel. Table 16 shows the computed parameters

Table 16: DC link capacitor parameters

Parameter	Value
Capacitance	1250 uF*2 = 2500 uF
Current capacity	255A*2 = 510 A_{rms}
Weight	14*2 = 28 kg
Volume	2*(21.5 cm*34 cm*11.7 cm) = 17000 cm^3

5.3.3 H-Bridge

For the SiC full bridge, 2 half bridge SiC Modules (1200 V, 800 A) [47] can be selected. The weight and volume are as shown in Table 17.

Table 17: SiC full bridge parameters

Parameter	Value
Weight	1.45*2 = 2.9 kg
Volume	(3.46 cm*15 cm*16.6 cm)*2 = 1700 cm^3

Total Weight of Active Inductor System without heat-sink = 171 kg

Total Volume of Active Inductor System without heat-sink = 68700 cm^3

It can be seen that the total weight and volume is lesser than that of 0.1 p.u. and 0.01 p.u. passive inductor. The Active Inductor will have additional weight and volume because of heat-sink which can be determined after loss analysis has been done. Moreover, there will be additional weight because of packaging all the components. The heat sink design can be done after loss analysis has been done.

5.4 Loss analysis

5.4.1 Passive inductor losses

There are two components of losses in passive inductor, core losses and winding losses. The losses in 0.1 p.u. inductor are:

- Inductor core losses:

Current Ripple, $\Delta I = 80$ A

$$\Delta B = \frac{L.\Delta I}{n.A_c} = 0.2 \text{ T} \quad (55)$$

From [60], – At 400 Hz, 0.2 T, Core Losses = 1 W/kg

Total core losses =1583 W

- Inductor winding losses:

$$\text{Resistance} = \rho \frac{l}{a} = 177.9*10^{-6} \quad (56)$$

I^2R losses = 18 W

Hence, total 0.1 p.u. passive inductor losses = 1.6 kW

The losses in 0.01 p.u. passive inductor are:

- Inductor core losses:

Current ripple, ΔI = 800 A, from (55)

$$\Delta B = \frac{L.\Delta I}{n.A_c} = 1 \text{ T}$$

From Figure 59 – At 400 Hz, 1 T, core losses = 6 W/kg

Core losses = 2581 W

- Inductor winding losses:

$$\text{Resistance} = \rho \frac{l}{a} = 55.3*10^{-6}$$

I^2R losses = 6 W

Hence, total 0.01 p.u. passive inductor losses = 2.5 kW

5.4.2 Active inductor losses

Assuming 40 kHz switching, DC Bus Voltage = 500 V, RMS Current = 300 A

- Switching losses – Turn On + Turn Off Losses

  From [47] the turn on and turn off loss per switch can be found.

  Turn on losses = 15 mJ/pulse

  Turn off losses = 15 mJ/pulse

  Total Switching losses $= 4.\left(Loss_{T_{off}} + Loss_{T_{on}}\right) * f_{switch} = 4.8$ kW (57)

- MOSFET R_{dson} losses

  $R_{DS-on} = 2.3$ mΩ

  R_{DS-on} Losses = 500 W

- MOSFET on-state drop losses

  $V_{DS-on} = 0.75$ V

  On state drop losses = 495 W

- Capacitor ESR losses

  ESR = 0.67 mΩ

  Capacitor losses = 36.5 W

- Inductor core losses

  $\Delta I = 100$ A

  From (55), ΔB = 0.25 T

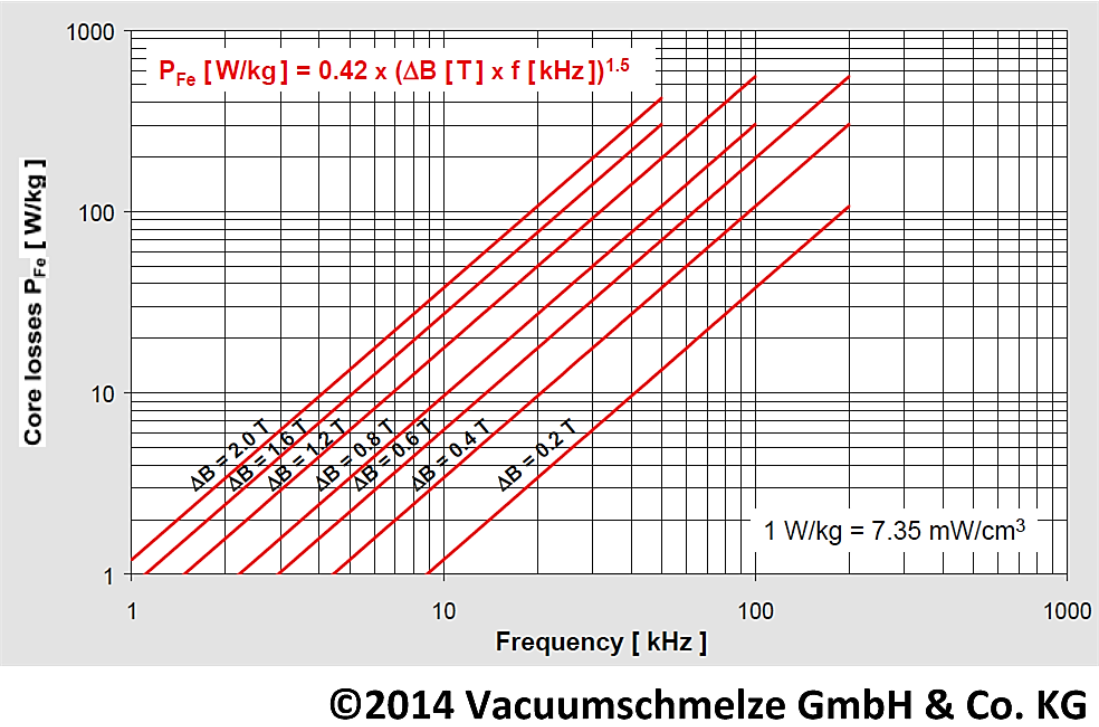

Figure 59: Nanocrystalline core (Vitoperm) core loss curves. Reprinted with permission from [61]

From Figure 59 – At 50 kHz and 0.25 T, Core losses = 15 W/kg

Core losses = 2.1 kW

- Inductor winding losses

  Resistance = $19.35*10^{-6}$ Ω

  I^2R Losses = 2 W

  Total Active Inductor losses = 7.9 kW

  Table 18 summarizes the losses in inductors considered.

Table 18: Loss analysis

Losses	Values
0.1 p.u. Passive inductor	1.6 kW
0.01 p.u. Passive inductor	2.5 kW
0.1 p.u. Active Inductor	7.9 kW

5.4.3 Heat sink

Another major concern for the adoption of Active Inductor is that the size of heat sink could become large. An analysis to calculate the heat sink is done after loss analysis. Thermal resistances of the contacts can be used to calculate junction temperature, T_j from (58).

$$\frac{T_j - T_a}{P_D} = \theta_{jc} + \theta_{ch} + \theta_{ha} \tag{58}$$

where P_D is derived from Loss analysis; θ_{jc} is junction to case thermal resistance, θ_{ha} is case to heat sink thermal resistance; θ_{ch} is heat sink to air thermal resistance.

Since junction to case contact is divided between 10 switches, θ_{jc} = 0.012. Also the parameter, T_j < 150°C & T_a = 25°C. Selecting T_j = 150°C and putting in (58)

$$\frac{T_j - T_a}{P_D} = 0.0133$$

From (58)

$\theta_{ch} + \theta_{ha}$ = 0.013 (Divided among 10 switches)

$\theta_{ch} + \theta_{ha}$ = 0.13 (For the complete module)

$\theta_{ha} = 0.08\ ^{o}C/W$ [62]

Hence, $\theta_{ha} = 0.05\ ^{o}C/W$ From table 19 [63], it can be found that, there are thermal compounds which fit the criterion. Table 19 summarizes the heat sink parameters.

Table 19: Heat sink design parameters

Parameter	Value
Weight of heat sink	4.5 kg
Volume of heat sink	18 cm*12 cm*10 cm = 2000 cm^3
Weight of blower	5 kg
Size of blower	12 cm*12 cm*4 cm = 576 cm^3
Total weight	9.5 kg
Total volume	2576 cm^3

Figure 60 shows that the filter inductor has the maximum weight percentage in the Active Inductor. Hence, for such an application, once the inductor size has been shrunk considerably, the total weight comes down automatically. Once the heat-sink design is completed, the actual weight and size of the Active Inductor can be calculated as shown in Figure 61.

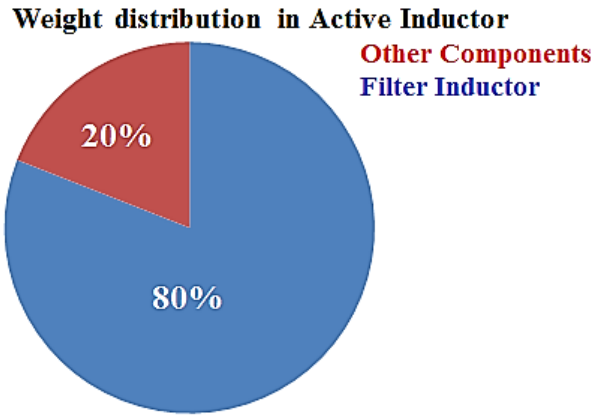

Figure 60: Weight distribution of Active Inductor

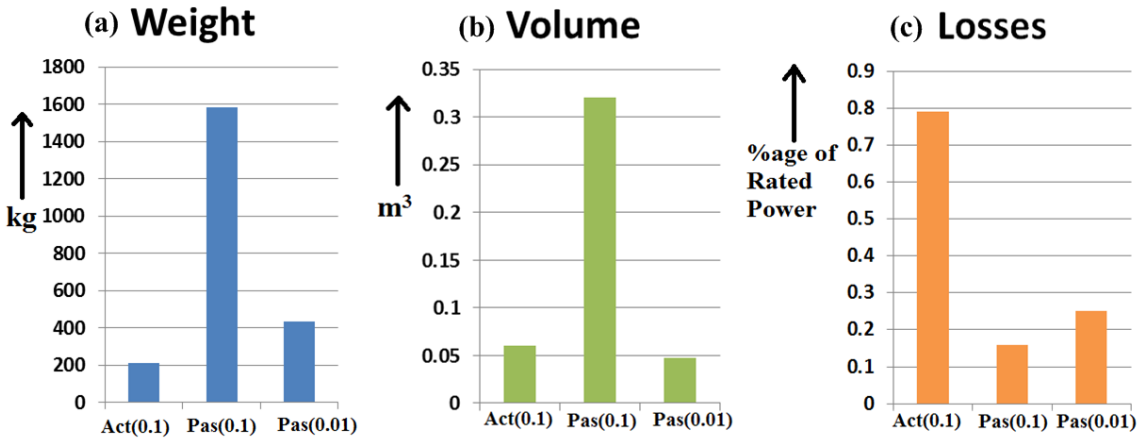

Figure 61: Weight, loss and size analysis

It can also be seen from Figure 61(a) that the Active Inductor is significantly smaller compared to 0.1 p.u. passive inductor and comparable to 0.01 p.u. inductor. Also from Figure 61(b), the weight of Active Inductor is lower than both the passive inductors. It can be seen from Figure 61(c) that although the losses are higher for the Active Inductor, it is less than 1% for the ASD power rating. Moreover, switching losses

constitute a major part of the losses and a ZVS turn-on method can be used to significantly reduce them.

5.5 Conclusion

A size, weight and loss analysis for both passive and Active Inductor is done. A heat sink design was done after loss analysis to make more accurate analysis of the Active Inductor. It is proven that the Active Inductor can achieve an inductance value of 0.1 p.u. passive inductor while having a similar weight/volume compared to the 0.01 p.u. passive inductor. This occurs because it is a small inductance value carrying a DC current with lower current ripple than the 0.01 p.u. passive inductor.

6. CONCLUSION AND FUTURE WORK

6.1 Summary

Consistent increase in power density of power converters has been a requirement in modern industrial plants. A passive inductor is an essential component of such converters because of its harmonic filtering properties. However, it tends to be bulky for high power ratings, increasing the weight/volume, rendering it unfavorable for industry. Moreover, passive inductors are not tunable and a dynamic behavior can improve transient system response. In response to these concerns, this thesis focused on design and analysis of Active Inductor to emulate a desired inductance value with a substantially reduced weight and volume.

The system design of the proposed topology is explained in detail and control strategy is described. The Active Inductor can replace a bulky passive inductor in LC filter of an ASD and LCL filter of a PV farm. Simulation and hardware results prove the concept and show better performance with good current and voltage quality. Apart from reducing size and weight, the Active Inductor is shown to improve response during faults and disturbances. Proper design of the inductor can prevent overvoltage in the DC link of an ASD during capacitor switching transient and assist in LVRT during grid disturbances in PV farm inverter.

A weight, size and loss analysis compared the passive inductors with the Active Inductor pertinent to the ASD system. The Active Inductor was found to be significantly lighter and smaller than the passive inductor with same per unit inductance and

comparable in weight/volume with the passive inductor of lower per unit rating. Therefore, it can be concluded that the proposed topology was able to realize the benefits of higher per unit inductance while having the same compactness as lower per unit inductance.

6.2 Future work

Future work would be done to explore the following:

- An analysis of cost/watt of the system.
- Evaluation of the component reliability of the system with varying conditions like operation at increased temperatures.
- EMI filter design for the proposed topologies.
- Conducting a higher power experiment to realize the practical increment in power density.
- Evaluating the actual size of the passive inductors with electromagnetic design softwares like JMAG.

REFERENCES

[1] U.S. Energy Information Administration(EIA),"Annual Energy Outlook," March 2009. Available: http://www.eia.gov/oiaf/aeo/pdf/0383(2009).pdf.

[2] P. Waide and C. U. Brunner, International Energy Agency(IEA), "Energy-Efficiency Policy Opportunities for Electric Motor-Driven Systems," 2011. Available: http://www.iea.org/publications/freepublications/publication/EE_for_ElectricSystems.pdf.

[3] R. Campos, IMS Research(IHS), "The World Market for Low Voltage AC & DC Motor Drives," November 2012. Available: http://www.imsresearch.com/products-services/pr-detail.php?pr_id=3244.

[4] M. Salama, "Lightweight materials for deepwater offshore structures," in *Offshore Technology Conference*, 1986.

[5] A. Fakhrul-Razi, A. Pendashteh, L. C. Abdullah, D. R. A. Biak, S. S. Madaeni, and Z. Z. Abidin, "Review of technologies for oil and gas produced water treatment," *Journal of Hazardous Materials,* vol. 170, pp. 530-551, 10/30/ 2009.

[6] TE Connectivity Ltd.,"Solutions for Offshore and Commercial Marine," 2012. Available: http://www.te.com/content/dam/te/global/english/tradeshow/Topsides2012/solutions-brochure-commercial-offshore-marine.pdf.

[7] K. H. Milo Hyde, "Energy Savings from Application of Variable Speed Drive (VSD) Motor Controllers in U.S. Navy Ships " in *ASNE Conference Proceedings.*, 2010.

[8] J. T. Raimund Rolfes, Richard Degenhardt, Hubert Temmen, Philipp Bürmann, Janos Juhasz, "New design tools for lightweight aerospace structures.," *Proceedings of the Seventh International Conference on Computational Structures Technology, Lisbon, Portugal,* 2004.

[9] J. Greenberg, "Are permanent magnet drilling motors the next generation? Manufacturers still disagree," Drilling Rig Equipment, Sepetember 2008. Available: http://drillingcontractor.org/dcpi/dc-septoct08/DC_Sept08_DrillingMotors.pdf.

[10] V. R. Stefanovic, "Trends in AC Drive Applications," *ELEKTRONIKA ELECTRONICS,* p. 10, 2000.

[11] T. Ericsen, "Engineering "Total Electric Ship"," presented at the Petroleum and Chemical Industry Technical Conference, 2007. PCIC '07. IEEE, 2007.

[12] H. S. Krishnamoorthy, P. N. Enjeti, I. J. Pitel, and J. T. Hawke, "New medium-voltage Adjustable Speed Drive (ASD) topologies with medium-frequency transformer isolation," in *Power Electronics and Motion Control Conference (IPEMC), 2012 7th International*, 2012, pp. 814-819.

[13] B. Singh, B. N. Singh, A. Chandra, K. Al-Haddad, A. Pandey, and D. P. Kothari, "A review of three-phase improved power quality AC-DC converters," *Industrial Electronics, IEEE Transactions on,* vol. 51, pp. 641-660, 2004.

[14] ABB Ltd., "Special Report – Motors & Drives," 2004. Available: http://www05.abb.com/global/scot/scot271.nsf/veritydisplay/97051077deb4950fc1256ea6004ffac5/$file/motors%20and%20drives.pdf.

[15] ABB Ltd., "Offshore Drilling Vessels:Total electrical systems for safe, efficient and environmental drilling operations," 2012. Available: http://www05.abb.com/global/scot/scot293.nsf/veritydisplay/ccf4f40a1062f74bc12577290036aaca/$file/abb%20drilling%20vessel%20brochure_lowres.pdf.

[16] Schlumberger Ltd., "Variable Speed Drives," 2011, Available: http://www.slb.com/services/production/artificial_lift/surface_equipment/~/media/Files/artificial_lift/brochures/vsd_brochure.ashx.

[17] European Wind Energy Association(EWEA), "The European offshore wind industry - key trends and statistics," 2012. Available: http://www.ewea.org/fileadmin/files/library/publications/statistics/European_offshore_statistics_2012.pdf.

[18] X. Sun, D. Huang, and G. Wu, "The current state of offshore wind energy technology development," *Energy,* vol. 41, pp. 298-312, 2012.

[19] C. H. Ng, M. A. Parker, L. Ran, P. J. Tavner, J. R. Bumby, and E. Spooner, "A Multilevel Modular Converter for a Large, Light Weight Wind Turbine Generator," *Power Electronics, IEEE Transactions on,* vol. 23, pp. 1062-1074, 2008.

[20] S. S. Gjerde, P. K. Olsen, and T. M. Undeland, "A transformerless generator-converter concept making feasible a 100 kV low weight offshore wind turbine Part II - The converter," in *Energy Conversion Congress and Exposition (ECCE), 2012 IEEE*, 2012, pp. 253-260.

[21] Solar Energy Industries Association(SEIA), "U.S. Solar Market Insight: 2010 Year in Review," 2010. Available: http://www.seia.org/sites/default/files/us-solar-market-insight-report-q1-2011-120627093305-phpapp01.pdf.

[22] S. Essakiappan, H. S. Krishnamoorthy, P. Enjeti, R. S. Balog, and S. Ahmed, "A new control strategy for megawatt scale multilevel photovoltaic inverters under partial shading," in *Power Electronics for Distributed Generation Systems (PEDG), 2012 3rd IEEE International Symposium on*, 2012, pp. 336-343.

[23] E. Koutroulis and F. Blaabjerg, "Methodology for the optimal design of transformerless grid-connected PV inverters," *Power Electronics, IET,* vol. 5, pp. 1491-1499, 2012.

[24] J. W. Kolar, J. Biela, S. Waffler, T. Friedli, and U. Badstuebner, "Performance trends and limitations of power electronic systems," in *Integrated Power Electronics Systems (CIPS), 2010 6th International Conference on*, 2010, pp. 1-20.

[25] J. W. Kolar, J. Biela, and U. Badstubner, "Impact of power density maximization on efficiency of dc-dc converter systems," in *Power Electronics, 2007. ICPE '07. 7th Internatonal Conference on*, 2007, pp. 23-32.

[26] ABB Ltd., "ACS 6000 variable speed drive system improves icebreaker's manoeuvrability and operability," 2011. http://www05.abb.com/global/scot/scot216.nsf/veritydisplay/8e623440dd382a37c12578cd00465abc/$file/CS_US%20Coast%20Guard_RevA_lowres.pdf.

[27] H. Mirzaee, S. Bhattacharya, R. Sei-Hyung, and A. Agarwal, "Design comparison of 6.5 kV Si-IGBT, 6.5kV SiC JBS diode, and 10 kV SiC MOSFETs in megawatt converters for shipboard power system," in *Electric Ship Technologies Symposium (ESTS), 2011 IEEE*, 2011, pp. 248-253.

[28] W. M. Grady, M. J. Samotyj, and A. H. Noyola, "Survey of active power line conditioning methodologies," *Power Delivery, IEEE Transactions on,* vol. 5, pp. 1536-1542, 1990.

[29] P. N. Enjeti, W. Shireen, P. Packebush, and I. J. Pitel, "Analysis and Design of a New Active Power Filter to Cancel Neutral Current Harmonics in Three-Phase Four-Wire Electric Distribution Systems," *Industry Applications, IEEE Transactions on,* vol. 30, p. 1565, 1994.

[30] L. Asiminoaei, E. Aeloiza, P. N. Enjeti, and F. Blaabjerg, "Shunt Active-Power-Filter Topology Based on Parallel Interleaved Inverters," *Industrial Electronics, IEEE Transactions on,* vol. 55, pp. 1175-1189, 2008.

[31] R. Cuzner, D. Drews, W. Kranz, A. Bendre, and G. Venkataramanan, "Power-Dense Shipboard-Compatible Low-Horsepower Variable-Frequency Drives," *Industry Applications, IEEE Transactions on,* vol. 48, pp. 2121-2128, 2012.

[32] T. Kerekes, R. Teodorescu, P. Rodriguez, G. Vazquez, and E. Aldabas, "A New High-Efficiency Single-Phase Transformerless PV Inverter Topology," *Industrial Electronics, IEEE Transactions on,* vol. 58, pp. 184-191, 2011.

[33] S. Harb and R. S. Balog, "Single-phase PWM rectifier with power decoupling ripple-port for double-line-frequency ripple cancellation," in *Applied Power Electronics Conference and Exposition (APEC), 2013 Twenty-Eighth Annual IEEE*, 2013, pp. 1025-1029.

[34] S. Harb, M. Mirjafari, and R. S. Balog, "Ripple-port module-integrated inverter for grid-connected PV applications," in *Energy Conversion Congress and Exposition (ECCE), 2012 IEEE*, 2012, pp. 1115-1120.

[35] A. Elasser and T. P. Chow, "Silicon carbide benefits and advantages for power electronics circuits and systems," *Proceedings of the IEEE,* vol. 90, pp. 969-986, 2002.

[36] M. C. Smith, "Synthesis of mechanical networks: the inerter," in *Decision and Control, 2002, Proceedings of the 41st IEEE Conference on*, 2002, pp. 1657-1662 vol.2.

[37] Z. Qing-Chang, "Active capacitors: Concept and implementation," in *Industrial Electronics (ISIE), 2012 IEEE International Symposium on*, 2012, pp. 149-153.

[38] M. Pierzchala, M. Fakhfakh, and B. Rodanski, "A novel design of active inductors based on current controlled voltage sources," in *Symbolic and Numerical Methods, Modeling and Applications to Circuit Design (SM2ACD), 2010 XIth International Workshop on*, 2010, pp. 1-4.

[39] L. Gyugyi, "Power electronics in electric utilities: static VAR compensators," *Proceedings of the IEEE,* vol. 76, pp. 483-494, 1988.

[40] H. Fnato, Y. Chiku, and K. Harakawa, "Wireless power distribution with capacitive coupling excited by switched mode active negative capacitor," in *Electrical Machines and Systems (ICEMS), 2010 International Conference on*, 2010, pp. 117-122.

[41] B. J. Pierquet and D. J. Perreault, "A single-phase photovoltaic inverter topology with a series-connected power buffer," in *Energy Conversion Congress and Exposition (ECCE), 2010 IEEE*, 2010, pp. 2811-2818.

[42] A. Prasai and D. Divan, "Scaling the Dynamic Capacitor (D-CAP) to medium voltages," in *Energy Conversion Congress and Exposition (ECCE), 2010 IEEE*, 2010, pp. 158-165.

[43] H. Funato, A. Kawamura, and K. Kamiyama, "Realization of negative inductance using variable active-passive reactance (VAPAR)," *Power Electronics, IEEE Transactions on,* vol. 12, pp. 589-596, 1997.

[44] T. Ishikawa, H. Funato, T. Ohtaki, and K. Kamiyama, "Transmission power control using variable inductance with feedforward- and feedback-based power controllers," in *Power Electronics and Drive Systems, 1999. PEDS '99. Proceedings of the IEEE 1999 International Conference on*, 1999, pp. 46-51 vol.1.

[45] H. Funato and A. Kawamura, "Control of variable active-passive reactance (VAPAR) and negative inductance," in *Power Electronics Specialists Conference, PESC '94 Record., 25th Annual IEEE*, 1994, pp. 189-196 vol.1.

[46] J. A. Sabate, V. Vlatkovic, R. B. Ridley, F. Lee, and B. H. Cho, "Design considerations for high-voltage high-power full-bridge zero-voltage-switched PWM converter," in *Applied Power Electronics Conference and Exposition, 1990. APEC '90, Conference Proceedings 1990., Fifth Annual*, 1990, pp. 275-284.

[47] R. A. Wood and T. E. Salem, "Evaluation of a 1200-V, 800-A All-SiC Dual Module," *Power Electronics, IEEE Transactions on,* vol. 26, pp. 2504-2511, 2011.

[48] AVX Corporation, "High Power Capacitors For Power Electronics," 2014, Available: http://www.avx.com/docs/masterpubs/hipwrflm.pdf.

[49] J. Long, M. McHenry, D. P. Urciuoli, V. Keylin, J. Huth, and T. E. Salem, "Nanocrystalline material development for high-power inductors," *Journal of Applied Physics,* vol. 103, pp. 07E705-07E705-3, 2008.

[50] Toshiba Ltd.,"Adjustable Speed Drives," 2014, Available: https://www.toshiba.com/tic/datafiles/ASD_Products_Brochure.pdf.

[51] B. Horvath, TMGE Automation Systems, "TM-GE MV Drives," November 2004. Available: http://www.wmea.net/Technical%20Papers/GE%20Medium%20Voltage%20Drives.pdf.

[52] N. Mohan and T. M. Undeland, *Power electronics: converters, applications, and design*: John Wiley & Sons, 2003.

[53] J. L. Duran-Gomez and P. N. Enjeti, "A new approach to mitigate nuisance tripping of PWM ASDs due to utility capacitor switching transients (CSTs)," *Power Electronics, IEEE Transactions on,* vol. 17, pp. 799-806, 2002.

[54] T. Erika and D. G. Holmes, "Grid current regulation of a three-phase voltage source inverter with an LCL input filter," *Power Electronics, IEEE Transactions on,* vol. 18, pp. 888-895, 2003.

[55] Y. Yang and F. Blaabjerg, "Synchronization in single-phase grid-connected photovoltaic systems under grid faults," in *Power Electronics for Distributed Generation Systems (PEDG), 2012 3rd IEEE International Symposium on*, 2012, pp. 476-482.

[56] R. W. Erickson and D. Maksimovic, *Fundamentals of power electronics*: Springer, 2001.

[57] J. Richmond, S. Leslie, B. Hull, M. Das, A. Agarwal, and J. Palmour, "Roadmap for megawatt class power switch modules utilizing large area silicon carbide MOSFETs and JBS diodes," in *Energy Conversion Congress and Exposition, 2009. ECCE 2009. IEEE*, 2009, pp. 106-111.

[58] M. S. Rylko, B. J. Lyons, J. G. Hayes, and M. G. Egan, "Revised Magnetics Performance Factors and Experimental Comparison of High-Flux Materials for High-Current DC-DC Inductors," *Power Electronics, IEEE Transactions on,* vol. 26, pp. 2112-2126, 2011.

[59] Wima Capacitors, "DC-Link Capacitors," 2011, Available: http://www.mouser.com/pdfDocs/WIMA_DC_Link_Capacitors.pdf.

[60] JFE Steel Corporation, "JFE Super Cores - Magnetic Property Curves," 2014, Available: http://www.jfe-steel.co.jp/en/products/electrical/catalog/f2e-001.pdf.

[61] Vacuumschmelze GmbH & Co. KG, "*Tape-Wound Cores for Magnetic Amplifier Chokes - Nanocrystalline VITOPERM 500 Z,"* 2014, Available: http://www.vacuumschmelze.com/fileadmin/documents/broschueren/kbbrosch/PKVP500Z_10.pdf

[62] Wakefield-Vette, "Heat Sinks," 2014, Available: http://www.wakefield-vette.com/Portals/0/resources/datasheets/392.pdf.

[63] Laird Technologies, "Tgrease 980," 2014, Available: http://www.abcpol.pl/download/materialy-termoprzewodzace/tgrease-980.pdf.